Wen et al. Chem. Biol. Technol. Agric. (2023) 10:142
https://doi.org/10.1186/s40538-023-00511-7

Chemical and Biological Technologies in Agriculture

RESEARCH

Open Access

Comprehensive transcriptomics and metabolomics revealed the antifungal mechanism of *Cymbopogon citratus* essential oil nanoemulsion against *Fusarium solani*

JinRui Wen[1], HongXin Liao[1], HongYan Nie[1], CuiQiong Ling[1], LiYan Zhang[1], FuRong Xu[1] and Xian Dong[1*]

Abstract

Background *Fusarium solani* (*F. solani*) is the main pathogen causing root rot of *Panax notoginseng* (Burk.) F. H. Chen (*P. notoginseng*). *Cymbopogon citratus* (DC.) Stapf (*C. citratus*) essential oil (EO) is a mixture of various active ingredients with good antifungal effects and no residue. However, due to its hydrophobicity and oxidation, its bioavailability is low.

Results In this study, EO was made into a nanoemulsion using Tween-80 and anhydrous ethanol by ultrasonication. The antifungal activity of the traditional emulsion (TEO) and *C. citratus* nanoemulsion (NEO) was compared by measuring the effects on spores and mycelia and in vivo assays. The components of EO, TEO, and NEO were analyzed by GC—MS, and the inhibitory mechanism of the emulsion against fungi was revealed by combining transcriptomics and metabolomics. The prepared NEO was a clear and transparent homogeneous liquid with a particle size of 15.86 ± 1.96 nm. It was an oil-in-water nanoemulsion and maintained good stability in different environments. The contents of antifungal components such as citronellal and linalool in NEO were significantly higher than those in TEO. The antifungal effect of NEO against *F. solani* was increased by 8 times compared with that of TEO. Through transcriptomic and metabolomic analyses, it was found that both NEO and TEO inhibited the fungi by destroying the cell membrane, thereby affecting the ribosome, meiosis and TCA cycle of the fungi, and NEO had a deeper effect than TEO. NEO also inhibited the gene expression of the CYR1 enzyme and decreased the amount of D-trehalose, thus inhibiting the germination of spores and thereby affecting the growth of mycelia.

Conclusions This study not only solved the problem of EO insoluble in water and low bioavailability but also greatly improved the antifungal activity, revealing the antifungal mechanism and the reason for the enhancement of NEO activity. It provides theoretical research for further development and utilization of EO to produce environmentally friendly pesticides or fertilizers and alleviate root rot of medicinal plants.

Keywords Nanoemulsion, Meiosis, TCA cycle, Ribosome, Botanical pesticides

*Correspondence:
Xian Dong
dongxian_1655129@163.com
Full list of author information is available at the end of the article

Graphical Abstract

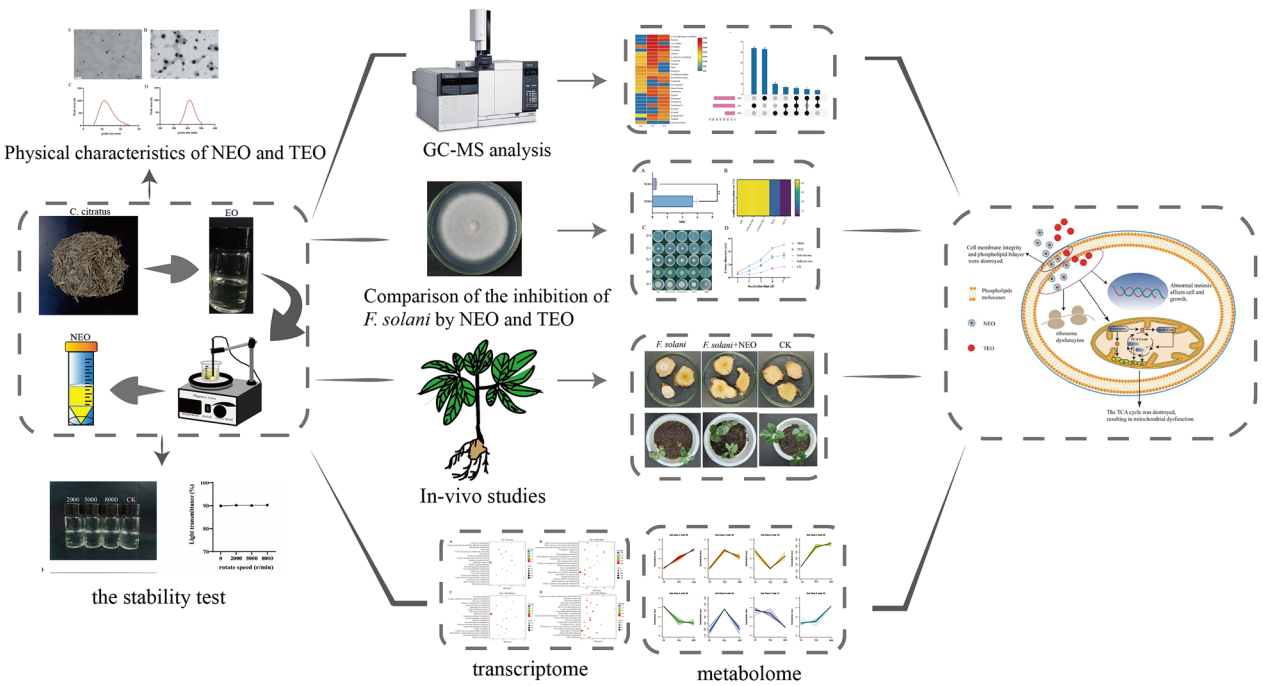

Background

P. notoginseng is a traditional perennial herb of Araliaceae that is often used to treat coronary heart disease and cardiovascular diseases [1]. This herb is widely used in medicine and health care products and has great market demand. However, due to its special planting pattern and environmental factors, continuous cropping obstacles are serious [2]. Root rot causes cracking and decay of the main medicinal organ, the rhizome, which seriously restricts the quality and yield of *P. notoginseng* [3]. Studies have shown that the occurrence and development of *P. notoginseng* root rot are closely related to the proliferation of disease-causing pathogens. There are many kinds of pathogenic microorganisms, from fungi to bacteria to nematodes, among which fungi are the main ones [4]. According to previous research, the main pathogenic microorganisms of *P. notoginseng* root rot disease include *Pseudomonas sp.* [5], *Fusarium oxysporum* (*F. oxysporum*) [6], *F. solani* [7], *Cylindrocarpon destructans*, *Achromobacter marplatensis*, and *Rhizoctonia solani* [8]. Among them, *F. solani* is a filamentous pathogenic fungus widely distributed in the world and is one of the main pathogens causing root rot of *P. notoginseng* [7].

Currently, the prevention or treatment of this disease mainly depends on crop rotation combined with chemical fungicides (such as carbendazim, hymexazol, and chlorothalonil) [9]. Chemical control plays an important role in the prevention and treatment of this disease, but chemical synthetic fungicides can cause great side effects while sterilizing. The long-term application of a large number of chemical fungicides and their unreasonable use will not only make pathogenic fungi resistant to pesticides but also cause great harm to the natural environment and human health [10]. Therefore, it is urgent to find natural fungicides with low toxicity, high efficiency, and no residue. Plant EO is a very important secondary metabolic compound that exists in various tissues, such as the flowers, leaves, and roots of plants [11]. It is mostly liquid at room temperature and highly volatile with a strong aroma and smell. Plant EO has become a research hotspot in the field of agricultural disease prevention and control due to its excellent antimicrobial activity, good biocompatibility, and abundant sources [12]. The EO of *C. citratus* is a natural plant metabolite with insecticidal and antifungal activities [13]. Previous studies have shown that EO can affect the metabolism of fungi and destroy cell walls, thus achieving antifungal effects [14]. EO has an obvious inhibitory effect on various pathogens causing root rot of *P. notoginseng* and has great potential to be developed as a green pesticide. However, in practical applications, the hydrophobicity and volatility of EO lead to its low bioavailability and cannot fully exert its

biological activity. Therefore, it is necessary to construct a delivery system to improve the hydrophobicity and reduce the volatility of EO. Nanoemulsions are thermodynamically stable transparent (translucent) dispersions of oil and water stabilized with an interfacial film of surfactants and cosurfactants, and their droplet sizes are less than 100 nm [15]. Nanoemulsions have been widely used in the medical field due to their small particle size, rapid penetration of cell membranes, and easy targeting to tumor areas [16]. Similarly, nanoemulsions have become an important delivery system for hydrophobic pesticides due to their advantages of fine and uniform droplets, good physical stability, strong permeability, and high bioavailability [17]. As a new type of emulsion, nanoemulsions have different physical properties, antifungal effects, and different inhibitory mechanisms for various pathogens.

In this study, the EO of *C. citratus* was prepared into a nanoemulsion, and its stability was evaluated to compare the inhibitory effects of NEO and TEO on *F. solani* and clarify the antifungal advantages of NEO. The components of NEO, TEO, and EO were analyzed and compared to clarify the differences in components. The combined analysis of transcriptomics and metabolomics revealed the common antifungal mechanism of NEO and TEO on *F. solani* and their respective unique mechanisms. Based on these data, we hope to further study and develop NEO to replace chemical fungicides for the prevention and control of *P. notoginseng* root rot, reducing harm to the environment and human body.

Materials and methods

Plants and fungi

The *C. citratus* used in the experiment were purchased from the management department of Deyang Yuanzhi Medicinal Materials in Guandu District, Kunming City. The seeds of *P. notoginseng* were cultivated in sterile saprophytic soil. After germination, the seeds were cultured in a greenhouse at a temperature of 20 °C, relative humidity of 70 ± 10%, and photocycle of 14 h/day. Two-year-old *P. notoginseng* root rhizome was purchased from Shunqiao Business Department, Wenshan City, Yunnan Province.

The strain isolated from the diseased roots of *P. notoginseng* was inoculated on PDA medium and incubated in a microbial incubator at 28 °C. DNA was isolated using a fungal DNA isolation kit, and the target gene was sequenced and identified by the internal transcribed spacer (ITS) of the fungus. Primer sequences were ITS1 (5′-TCCGTAGAGAACCTGG-3′) and ITS4 (5′-TCCTCG CTTATGC-3′). Sequencing was completed by China Biotechnology Co., Ltd., and sequencing results were uploaded to GenBank. The BLAST alignment showed that these sequences were homologous to the sequence of *F. solani* MG24128, and the homology was 100%. The accession number in GenBank is OQ080021.1.

Preparation of *C. citratus* EO

One kilogram of dried *C. citratus* and distilled water were placed into a 10 L round bottom flask at a ratio of 1:8. After soaking for 10 h, the EO was distilled by steam distillation for 6–9 h. After removing water with anhydrous sodium sulfate, the collected EO was stored in a brown bottle and placed in a refrigerator at − 20 °C for further use [18].

Preparation of TEO

According to the reference [19] and with slight modification, the EO was dissolved in an aqueous solution of 2-DMSO-T (a mixture of 2% DMSO and 0.1% Tween-80 according to the required concentration) and then emulsified in an ice bath for 20 min for further use.

Preparation of NEO

Establishment of the EO microemulsion system

The Km value is the mass ratio of the surfactant and cosurfactant. A certain mass ratio (Km = 1, 2, 3) of surfactant (Tween-80) and cosurfactant (anhydrous ethanol) was weighed into a beaker, placed on a magnetic stirrer, and stirred for 5 min. The mixture was placed in an ice bath for ultrasonic treatment for 20 min (power: 300 W). Then, the total mass of the prepared mixed surfactant and oil phase was 4 g, and the mass ratios were 8:2, 6:4, 4:6, and 2:8. After mixing, the mixture was placed at room temperature for 15 min, and then distilled water was gradually added dropwise with a pipette and stirred while dripping. The operation was repeated until the solution changed from clear to turbid, and the state remained unchanged for 30 min. The amount of distilled water added was recorded at the critical point (repeated twice to take the average value), and the mass fraction of this component was calculated at the transition point. The mixed surfactant, EO, and distilled water were used as the three phases to make the three-phase diagram, and the area was calculated. The best EO microemulsion system was determined as Km = 2 and a surfactant:EO ratio of 8:2 [20].

Preparation of NEO

Tween-80 and anhydrous ethanol were added into a beaker at a 2:1 mass ratio, stirred in a magnetic agitator for 5 min, and then ultrasonicated in an ice bath for 20 min to produce mixed surfactants. EO and mixed surfactant were weighed in a beaker at a ratio of 1:4, stirred for 5 min, and then ultrasonicated in an ice bath for 20 min. After standing for 15 min, the mixture was

stirred, and water was added while stirring (EO:mixed surfactant:water = 1:4:4). After stirring for 5 min, the mixture was ultrasonicated in an ice bath for 20 min to obtain NEO.

Morphological observations and particle size analysis of the two emulsions

The two emulsions were diluted 10 times with deionized water, and the diluted emulsions were observed under a transmission electron microscope (JEM-1011, JEOL, Co. Ltd., Tokyo, Japan) for particle morphology. The particle size of the emulsions was measured by a laser particle size meter (90Plus PALS).

Stability of NEO

The stability of NEO was measured according to the reference [21] and with slight modification. The NEO was centrifuged, salt treated, acid–base treated, high-low temperature treated, and light treated, and then the transmittance was measured before and after the treatment.

$T = 10^{-A}$

(T: transmittance; A: absorbance).

Chemical composition analysis by gas chromatography–mass spectrometry (GC–MS)

The chemical components of EO, NEO, and TEO were analyzed through GC–MS (Agilent Technologies 7890B-5977B) according to our previously described method [22].

Comparison of antifungal activity between NEO and TEO

The minimum inhibitory concentration (MIC) of NEO and TEO was determined by the method published by our research group [12]. The initial concentration of NEO was 4 mg/mL, and the initial concentration of TEO was 25 mg/mL. In the 96-well plate, 150 μL spore suspension was first added, and then 50 μL emulsions of different concentrations was added. The solvent of the two emulsions (50 μL) was added as the negative control group, and 150 μL 1/3 PDA liquid + 50 μL water was the blank control.

Hyphal growth was measured according to the reference [23]. Under sterile operating conditions, the corresponding emulsion or solvent was added to the PDA to make the concentration of the emulsion or solvent reach 0.45 mg/mL. Each treatment had 5 replicates, and the colony growth diameter was measured every 24 h to obtain the growth curve of *F. solani.*

Conidial germination rate was measured according to the reference [24]. NEO and TEO were added to a sterile EP tube containing 1/3 PDA liquid medium and mixed well to an emulsion concentration of 0.45 mg/mL, and finally, an appropriate amount of spore suspension was added to a final concentration of 1×10^6/mL. Each treatment was repeated 3 times. The total number of spores and the number of germinated spores were counted by blood cell counting plates under a microscope.

$B = (C_1/C_0) \times 100\%$,

B: spore germination rate; C_1: the number of germinated spores; C_0: total number of spores.

Transcriptome and metabolome sequencing

Transcriptome and metabolomic analyses were performed on *F. solani* hyphae treated with NEO and TEO for 24 h and untreated and labeled as NEO, TEO, and EO, respectively, with 3 biological replicates in each group. Transcriptomic and metabolomic analyses were performed by MetWare Biotechnology Co. Ltd. (Wuhan, China). The de novo assembly of the transcriptome was generated using Trinity software (v.2.11.0). All assembled unigenes were annotated in the following databases: NR (NCBI nonredundant protein sequence), GO (Gene Ontology), KEGG (Kyoto Encyclopedia of Genes and Genomes), eggNOG (Gene Evolution Pedigree: Unsupervised Positive Homologous Group), Swiss-Prot (Artificially Annotated and Reviewed Protein Sequence Database), and Pfam (Protein Family). Unigenes with | log2Fold Change |≥1 and FDR < 0.05 were designated DEGs. To infer the hypothetical function of DEGs, we performed GO enrichment analysis using the top GO and KEGG pathways and enrichment analysis using clusterProfiler.

The metabolome was analyzed by ultra-performance liquid chromatography (UPLC) tandem mass spectrometry. The main and secondary MS data were qualitatively analyzed by using the self-compiled database MWDB (MetWare Biotechnology, Ltd.) to search the internal database. Differentially accumulated metabolites (DAMs) were screened according to the importance of projection variables (VIP) ≥ 1 and |log2(fold change)| ≥ 2. The function of DAM was further annotated using the KEGG compound database to determine the antifungal mechanism of NEO and NEO.

RT–PCR analysis

The purified RNA (1 μg) was reverse transcribed into first strand cDNA using a cDNA reverse transcription kit. The list of primers is shown in the attached table (primer map). A ChamQ SYBR qPCR main mixing kit (Vazyme) and C1000TouchTM thermal cycle system (Bio-Rad) were used for qRT–PCR. The relative transcription level was calculated by the 2-ΔΔCp method using actin as an internal reference gene. All experiments were conducted in triplicate.

In vivo experiment of *P. notoginseng*

The roots of *P. notoginseng* with uniform size were selected and cut into approximately 0.5 cm thick pieces after cleaning. After disinfection with alcohol and sodium hypochlorite, the pieces were placed in a plate covered with water agar. The 5 mm diameter of the fungal blocks was placed in the center of the *P. notoginseng* block was used as a positive control, and 3 μL of NEO at a concentration of 0.45 mg/mL was added to the bacterial block as a treatment group.

One-year-old *P. notoginseng* seedlings were selected, and 10 mL spore suspension at a concentration of 2×10^6/mL was added to the soil around the stem base of the plant as a positive control. NEO was mixed with an *F. solani* suspension to a final NEO concentration of 0.45 mg/mL as the treatment group, and 10 mL of sterile water was poured into the soil as the blank control [25]. Disease incidence (DI) = number of diseased plants/total number of plants × 100%

Disease status was graded as follows:

Grade 0: plants are healthy.

Grade 1: spots on the leaves of the plants.

Grade 2: wilting of the plant.

Grade 3: plant death.

Disease index $(Di) = 100 \times \sum(Dn \times Dg)/(Tn \times Mg)$.

Where *Dn* indicates the number of plants with the same disease level, *Dg* is the corresponding disease level, *Tn* is the total number of plants, and *Mg* is the highest disease level.

Statistical analysis

All experiments in this study were repeated three times, and the data shown are the mean ± SD (standard deviation). The results were subjected to one-way ANOVA (p value of ≤ 0.05), LSD (least-significant difference), and Tukey's multiple range test to determine significant differences in the average. These data were analyzed using the SPSS program version 19.0. The results were finally plotted using the Origin program version 2019b, Adobe Illustrator 2022 and GraphPad Prism 9.

Results

Establishment of the microemulsion system

We used 1/1000 Tween-80 and 20/1000 DMSO as emulsifiers to prepare TEO. While making NEO, Tween-80 was used as a surfactant, and anhydrous ethanol was used as a cosurfactant to obtain a mixed surfactant by mixing and stirring ultrasonically at different ratios. Mixed surfactant, EO, and distilled water were used as three phases to make a three-phase diagram with the origin, and the area was calculated. Through screening, the best EO microemulsion system was determined to be Km = 2, and the ratio of mixed surfactant to EO was 4:1. (Additional file 1: Fig. S1).

Physical characteristics of NEO and TEO

Nanoemulsions are a thermodynamically stable, isotropic, transparent, or translucent homogeneous dispersion system formed from water, oil, surfactant, and cosurfactant with a particle size of 1 ~ 100 nm [26]. Nanoemulsions are usually divided into three types, namely, oil-in-water nanoemulsions (O/W), water-in-oil nanoemulsions (W/O), and bicontinuous nanoemulsions (BCs). By measuring its conductivity, the NEO we produced was an oil-in-water nanoemulsion (O/W) [15].

Different sizes of subspherical smooth surfaces were observed in NEO and TEO through TEM, and it was clear that the particle size of NEO was significantly smaller than that of TEO (Fig. 1A, B). The average particle size of NEO was 15.86 nm, and that of TEO was 461.25 nm (Fig. 1C, D). The reduced particle size of NEO compared to TEO was attributed to sonication, and the smaller particle size of NEO could penetrate the fungal cell membrane more easily and thus greatly enhance its ability to inhibit the fungus.

Stability testing of NEO

The light transmission of NEO at different temperatures (− 20 °C, 4 °C, 30 °C, 40 °C), salt concentrations (1%, 3%, 5%), and rotational speeds (2000, 5000, 8000) was not significantly different from that of the control group, and no turbidity stratification was observed, showing good stability (Additional file 1: Fig. S2A, C, D). Turbidity and light transmission were decreased at pH 5 and 6 compared to the control group and stabilized at pH 7 and 8 (Additional file 1: Fig. S2B). The inhibition ability against *F. solani* was not significantly different from that of the control with NEO treated at different light levels (0, 30%, 60%, 90%) (Additional file 1: Fig. S3). All these results indicated that the formulated NEO was stable and has the potential to be used in the field.

Comparison of the inhibition of *F. solani* by NEO and TEO

To investigate the inhibitory effect of NEO and TEO on *F. solani*, we treated the spores and mycelium of *F. solani* with NEO and TEO, respectively, and the respective MIC values were measured. As seen from the figure, the MIC value of NEO was 0.81 mg/mL, which was significantly smaller than that of TEO (5.78 mg/mL) (Fig. 2A). The spores of *F. solani* were treated with the same concentration (0.45 mg/mL) of NEO and TEO. It can be clearly seen that the germination rate of spores

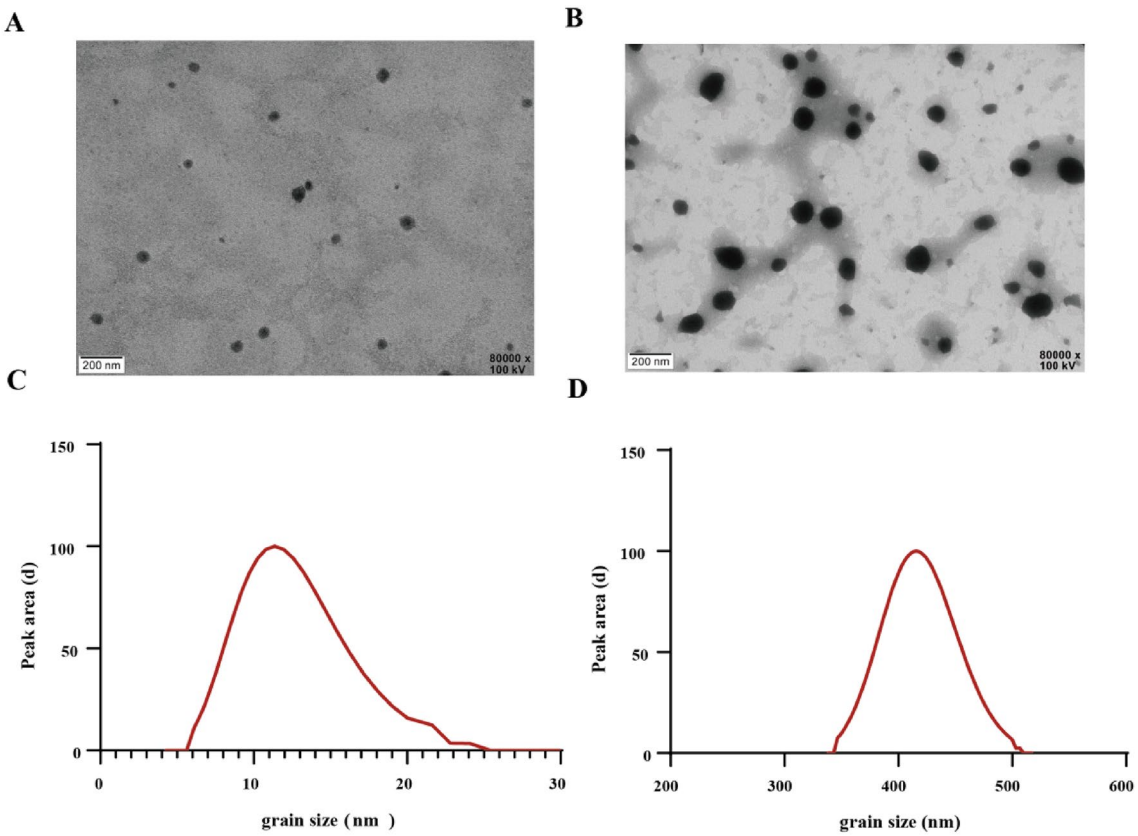

Fig. 1 Comparison of particle sizes of NEO and TEO. TEM diagrams of NEO (**A**) and TEO (**B**). Particle size diagrams of NEO (**C**) and TEO (**D**)

treated with NEO (8.86%) was significantly lower than that of TEO (34.57%) (Fig. 2B), and the growth rate and colony size of *F. solani* treated with NEO were significantly smaller than those treated with TEO (Fig. 2D). The spore germination rate and mycelial growth after treatment with the two solvents were not significantly different from those of the blank control, indicating that the solvents of the two emulsions had no antifungal activity. The enhanced antifungal activity of NEO compared to TEO could be related to the smaller particle size of NEO, and then the specific surface area was substantially increased, resulting in the increased contact area with the target protein and finally the increased antifungal effect of the active ingredient.

Chemical composition analysis of NEO and TEO

A total of 61 compounds were identified in the EO, including alcohols (47.05%), phenols (20.15%), olefins (19.09%), and aldehydes (10.09%). The main components were 3,7-cyclodecadiene-1-methanol (17.635%), geraniol (14.626%), and (−)-a-cadinol (12.695%) (Additional file 1: Fig. S4A). A total of 28 compounds were identified in NEO, including alcohols (41.60%), phenols (7.35%), aldehydes (35.28%), and olefins (7.42%). The main components were citronellal (34.28%), geraniol (18.38%), and citronellol (13.98%) (Additional file 1: Fig. S4B). A total of 57 components were identified in TEO, including alcohols (18.62%), aldehydes (16.78%), olefins (5.18%), and phenols (0.79%). The main components were citronellal (16.589%), nerol (5.806%), and carbonic acid, allyl 3-methylphenyl ester (3.93%) (Additional file 1: Fig. S4C).

There are 6 common components, linalool (El-Baky and Hashem, 2016), (+)-DELTA-CADINENE, γ-eudesmol [27], o-allylhydroxylamine, dl-citronellol acetate [28], and geranyl acetate [29] have been reported to have good antimicrobial activity. It can be seen from the heatmap of the main components (Fig. 3A) that the components of NEO and EO are similar, which proves that the preparation of NEO can better maintain the main components of the original EO, while the components of TEO fluctuate greatly compared with EO. Although the number of components in TEO is similar to that in EO, the main components are quite different from those in EO. At the same time, although NEO contains a small

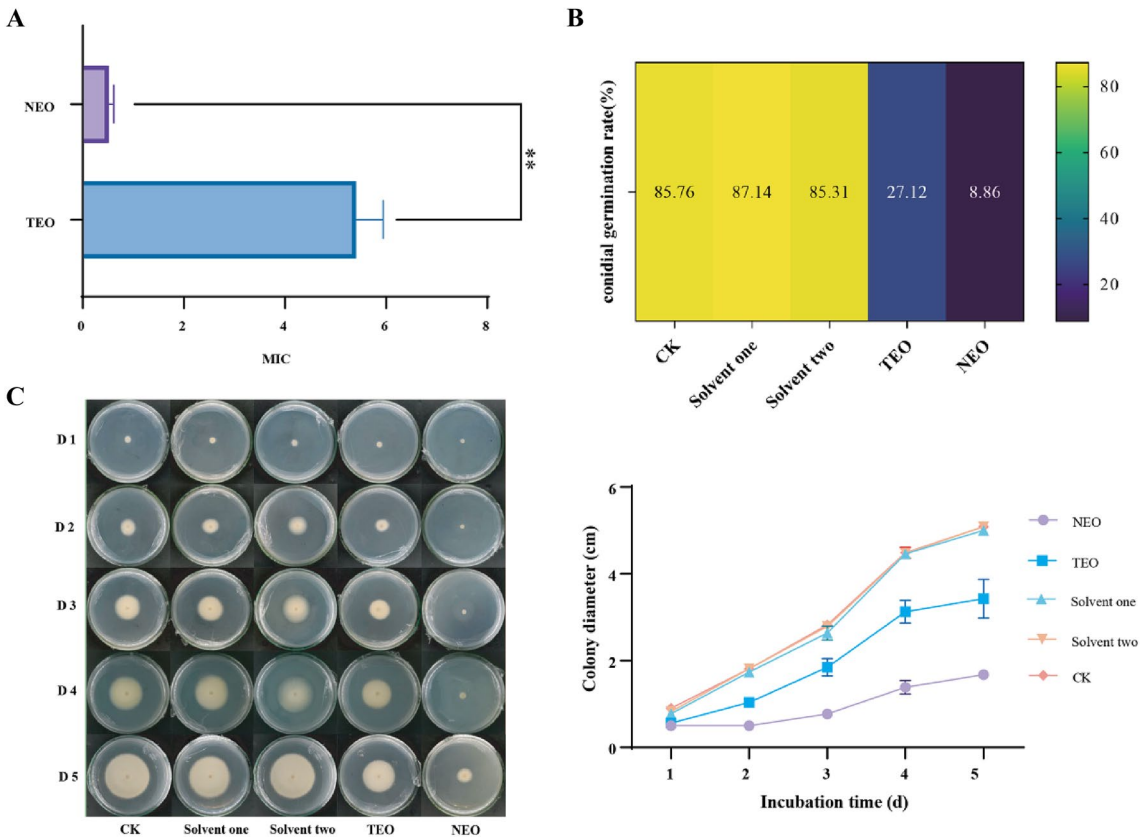

Fig. 2 Effects of different emulsions on spore germination and mycelia growth. Tween-80 and DMSO were used as solvent I, mixed surfactant was used as solvent II, and sterile water was used as CK. The MIC (**A**), spore germination (**B**), and hyphal growth (**C**, **D**) of TEO and NEO were compared. The TEO and NEO concentrations on hyphae and spores were 0.45 mg/mL. Solvent one included Tween-80 and DMSO. Solvent two included Tween-80 and alcohol. The values are presented as the mean of three replicates. Asterisks above the bars indicate significant differences at the 0.05 level according to Duncan's multiple range test

number of components, it retains the main components of EO (Fig. 3A, B).

Transcriptomic analysis after NEO and TEO treatment of *F. solani*

Gene expression profiles of the nine samples were analyzed by PCA (Additional file 1: Fig. S5A), and the results showed that the significant difference between TEO and CK was mainly in PC1 (59.16%), while the difference between NEO and CK was mainly in PC2 (12.8%). The Venn diagram shows (Additional file 1: Fig. S5B) that NEO and TEO have 2396 common DEGs. In addition, 2040 unique DEGs were found in CK vs. NEO, while 755 unique DEGs were found in CK vs. TEO. These unique 2040 DEGs obtained in CK vs. NEO might be the reason for the stronger inhibitory effect of NEO. A total of 5259 DEGs were analyzed in both groups of samples, of which 2055 were upregulated and 2330 were downregulated in CK vs. NEO; 1644 were upregulated and 1711 DEGs were downregulated in CK vs. TEO (Additional file 1: Fig. S5C, D). To verify the biological functions of the DEGs after NEO and TEO treatment, GO functional enrichment analysis was performed for the DEGs (Additional file 1: Fig. S6). The expression genes of the NEO treatment group and TEO treatment group were coconcentrated in organic acid transport, organic acid transmembrane transport, ribosome, ribosome subunit, peroxisome, large ribosome subunit, ribosome structural component, cytoplasmic ribosome, organic acid transporter activity, amino acid transporter activity, etc. Taken together, the DEGs of both the NEO and TEO treatment groups were mainly coenriched in ribosomes and organic acids. Ribosomes are the machinery of protein synthesis in cells, whose main function is to transfer genetic information into amino acid sequences and use amino acids to synthesize protein polymers [30]. Some organic acids, such as fumaric acid, L-malic acid, and citric acid, are intermediates in the oxidized tricarboxylic acid (TCA) cycle and play an important role in mitochondrial localization in eukaryotes [31].

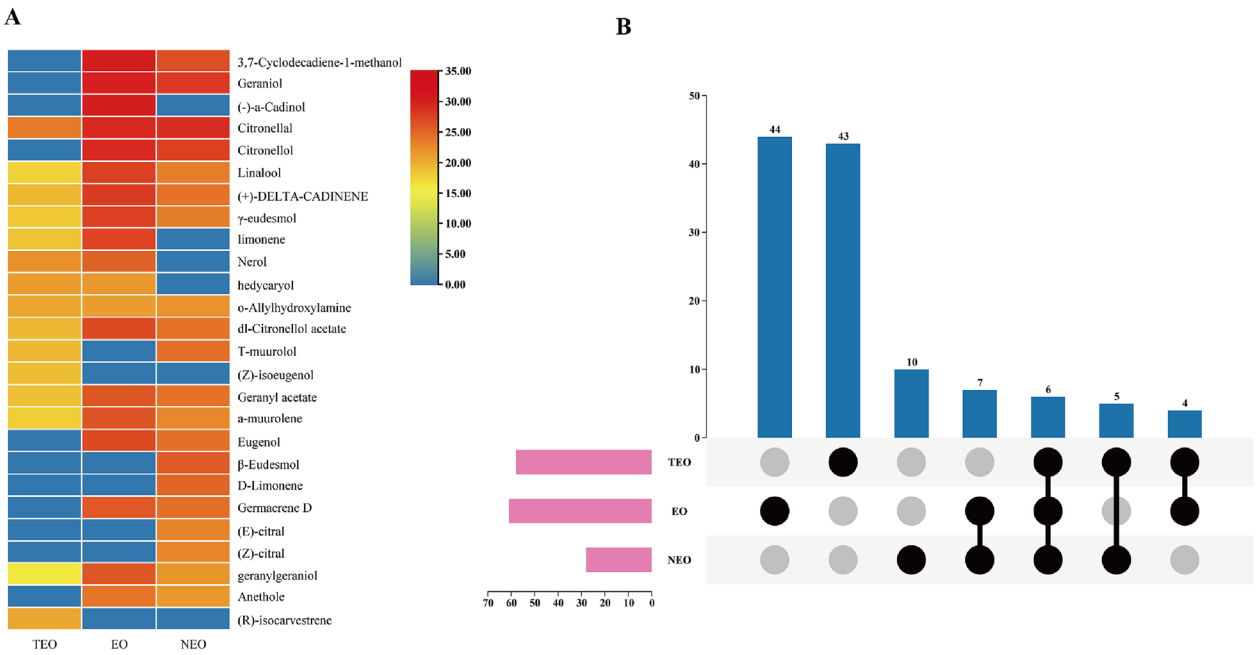

Fig. 3 The chemical constituent analyses of EO, NEO, and TEO were performed using GC—MS. **A** Clustering heatmaps for each of the three groups using the base log scale of the GC—MS peak area. **B** Upset diagram of the main chemical components in the three groups

Therefore, the two emulsions may affect the structure and function of ribosomes and other organelles in the cell. Compared with the TEO treatment group, the NEO treatment group showed more significant enrichment of DEGs in sphingolipid metabolism, membrane lipid decomposition, cellular lipid decomposition, intrinsic components of the mitochondrial membrane, and overall components of the mitochondrial membrane, indicating that NEO inhibited fungi by gradually dissolving fungal cell membranes, thus destroying mitochondria and ribosomes.

The KEGG database was used to annotate DEGs, and the top 20 pathways with the highest enrichment are shown in Fig. 4. The ribosome was upregulated jointly after NEO and TEO treatment, and there were more changes in differential genes in the NEO treatment group (Additional file 1: Fig. S7 B), which was consistent with the GO results. In addition, we found a codownregulated pathway (meiosis), which is not significant but still plays a significant role.

The changes in genes encoding corresponding enzymes in meiosis are shown in Additional file 1: Fig. S7A. *F. solani* was treated with two emulsions to jointly inhibit the expression of protein kinases such as checkpoint serine/threonine-protein kinase (Bub1), ser/thr/tyr protein kinase (Pad53), meiosis induction protein kinase (Ime2), and int carbon catabolite-derepressing protein kinase (Snf1). The decrease in Bub1 and Pad53 expression will make the genome of fungal cells unable to replicate and separate with high fidelity [32, 33]. Inhibition of Snf1 expression will lead to the failure of meiosis to stop fungal growth or even death [34], while the decrease in ime2 expression will seriously affect the mycelial growth and spore germination of fungi, which is consistent with the previous phenotypic results [35] (Fig. 2). NEO also inhibits the expression of adenylate cyclase (CYR1). The decrease in CYR1 expression leads to arrest in the G1 phase of the cell cycle. CYR1 is involved in the synthesis of cAMP, which can mediate the effect of glucose on gluconeogenesis and spore germination, thus inhibiting the mycelial growth and spore germination of fungi [36].

Peroxisome, oxidative phosphorylation, glutathione metabolism, and fatty acid biosynthesis were upregulated in the NEO treatment group (Fig. 4A). These results indicated that *F. solani* treated with NEO can resist the cytotoxicity caused by NEO through the oxysome, glutathione metabolism, and fatty acid biosynthesis and enhance the oxidative phosphorylation pathway to produce ATP for cell energy. Tyrosine metabolism, the pentose phosphate pathway, sucrose and starch metabolism, amino acid metabolism (histidine, glycine, serine, threonine), and other pathways were downregulated (Fig. 4B). This indicated that NEO treatment destroyed the energy metabolism of fungi, thus thwarting the energy source of fungi. Moreover, the downregulation of tyrosine metabolism reduces the production of pyomelanin-a mycotoxin, thereby reducing

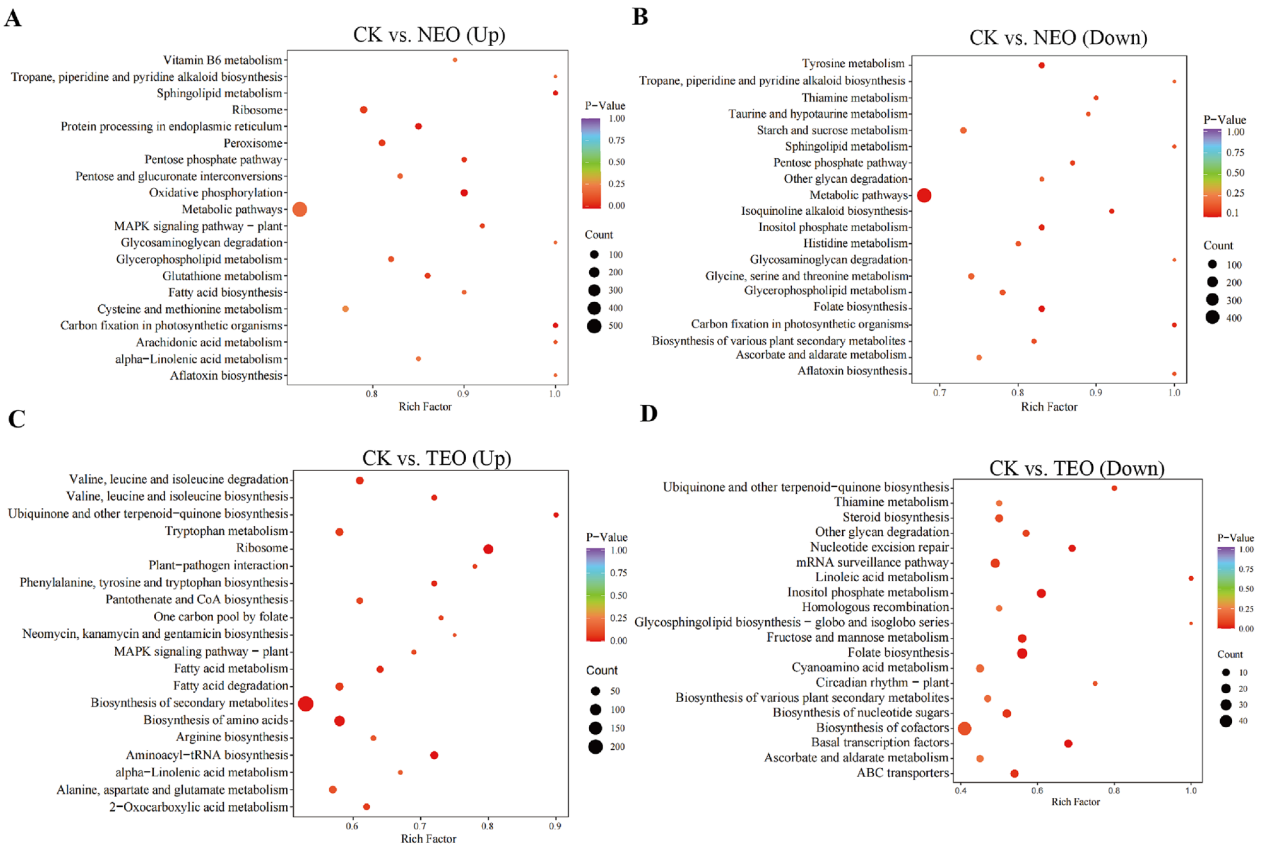

Fig. 4 The top 20 enrichment pathways of DEGs from KEGG analysis. **A** Up-regulated differential genes in CK vs. NEO; **B** Down-regulated differential genes in CK vs. NEO; **C** Up-regulated differential genes in CK vs. NEO; **D** Down-regulated differential genes in CK vs .TEO. The X-axis is the rich factor, and the Y-axis represents the name of the pathway. The bubble size represents the number of DEGs involved. The bubble color indicates the enrichment degree of the pathway. All treatments were consistent with the above

fungal virulence [37]. In addition, the downregulation of the pentose phosphate pathway reduces the production of a reducing agent (NADPH) and affects mitochondrial function, thereby inhibiting fungi [38].

However, the biosynthesis of secondary metabolites, amino acid biosynthesis (tryptophan, arginine, phenylalanine), and amino-tRNA biosynthesis in the TEO treatment group showed an upregulated trend (Fig. 4C). These results indicate that after TEO treatment, *F. solani* can synthesize secondary metabolites and proteins through abundant enrichment of secondary metabolite biosynthesis, amino acid biosynthesis, and amino-tRNA biosynthesis pathways to resist invasion. Moreover, basic transcription factors, biosynthesis of nucleotide sugars, and biosynthesis of cofactors were downregulated after TEO treatment (Fig. 4D). These results indicated that TEO treatment damaged DNA synthesis, transcription, and other processes of fungi and inhibited the biosynthesis of cofactors, resulting in the loss of most enzyme activities in fungi, thus inhibiting fungi.

Study on the metabolomics of *F. solani* hyphae treated with NEO and TEO

The mycelium of *F. solani* treated with NEO and TEO was extensively targeted for metabolomic analysis. In the PCA diagram, the three samples are clustered separately and far apart, which indicates that there is a large difference in metabolites among the three samples (Additional file 1: Fig. S8 A). The two comparisons (CK vs. NEO, CK vs. TEO) had 233 and 214 DAMs, respectively. Among them, 143 and 136 upward and 90 and 78 downward, respectively. The level of mycelial metabolites after NEO and TEO treatment showed a significant change (Additional file 1: Fig. S8B). Venn diagram analysis showed that 103 DAMs of CK vs. NEO and CK vs. TEO were coupregulated, which may be related to the resistance of pathogens, and 59 DAMs were codownregulated, which may be related to the inhibition of *F. solani*. In addition, 40 upregulated and 31 downregulated DAMs specific to CK vs. NEO may be the reason for the stronger antifungal activity of NEO (Additional file 1: Fig. S8C, D).

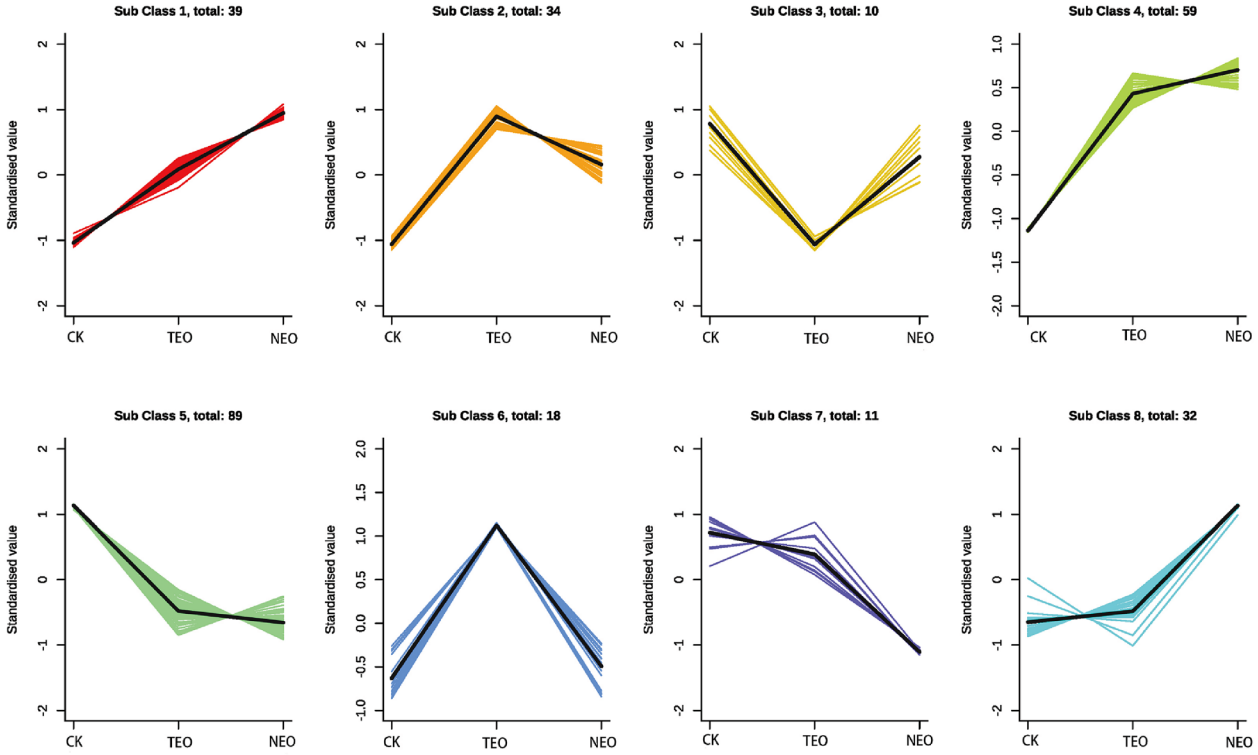

Fig. 5 K-means cluster of variation trends of the relative content of metabolites in different groups. The three treatments were CK, TEO, and NEO. The abscissa represents the grouping of samples, the ordinate represents the relative content of standardized metabolites, and the subclass represents the number of metabolites with the same change trend. All treatments were consistent with the above

We annotated the DAMs using the KEGG database. The top 20 pathways with the highest enrichment in the two comparison groups are shown in Additional file 1: Fig. S9. Nine metabolic pathways were coenriched after NEO and TEO treatment, including α-linolenic acid metabolism, drug metabolism-other enzymes, nucleotide metabolism, ABC transporter, caprolactam degradation, xylene degradation, tuberculosis, purine metabolism, and tyrosine metabolism. In the NEO treatment group, DAMs were mainly enriched in antibiotic synthesis, pyruvate metabolism, and amino acid metabolism. However, sphingolipid metabolism and glycolysis/gluconeogenesis were more enriched in the TEO treatment group.

To evaluate the change in metabolites between groups, the relative contents of all different metabolites identified according to the screening criteria in each group were standardized by Z score, and then K-means clustering analysis was performed (Fig. 5). In different groups, the concentration of metabolites gradually increased from low to high, such as subclass 1, subclass 4, and subclass 8, with a total of 130 metabolites, mainly nucleotides and their derivatives, amino acids and their derivatives, phenolic acids, organic acids, and flavonoids. The gradually reduced metabolites included subclass 5 and subclass 7, with a total of 100. These substances mainly include lipids, amino acids and their derivatives, organic acids, and phenolic acids. Among them, we found that the concentration of components related to cell membrane components decreased significantly (Additional file 1: Fig. S10A), indicating that the cell membrane of fungi was destroyed after two emulsion treatments, and the degree of NEO damage was deeper than that of the TEO treatment group, which was consistent with the previous GO results.

Combined analysis of the transcriptome and metabolome

To further explore the relationship between DEGs and DAMs in *F. solani* after NEO and TEO treatment, we conducted transcriptome and metabolome coexpression analysis of CK vs. NEO and CK vs. TEO. As shown in Fig. 6A and B, it can be clearly seen that significant coexpression pathways in the NEO treatment group included α-linolenic acid metabolism, arachidonic acid metabolism, pyruvate metabolism, thiamine metabolism, tyrosine metabolism, and phenylalanine metabolism. In the TEO treatment group, α-linolenic acid metabolism, valine, leucine and isoleucine biosynthesis, glycolysis/

gluconeogenesis, and tyrosine metabolism were significantly coexpressed.

We analyzed the coexpression network of the transcriptome and metabolome in the NEO treatment group and TEO treatment group, as well as the enriched pathways of the NEO treatment group and TEO treatment group. In the network diagram of NEO and TEO coenrichment, we found that some metabolites, such as L-tyrosine, 3,4-dihydroxyphenylacetic acid, and tyrosol, were linked to multiple genes, with a strong correlation (Fig. 7C), and the NEO treatment group had more expression than the TEO treatment group (Additional file 1: Fig. S10 C), in which L-tyrosine and 3,4-dihydroxyphenylacetic acid were downregulated metabolites. Melanin is synthesized by tyrosine under the action of tyrosine synthase, which can not only strengthen fungal cells but also promote the spore germination of fungi [37, 39]. 3,4-Dihydroxyphenylacetic acid can be converted into o-phenylquinone and then into melanin under the action of tyrosinase, and L-tyrosine and 3,4-dihydroxyphenylacetic acid can be downregulated after NEO and TEO treatment. As a result, melanin production is reduced, cell walls are weakened, and fungal spore germination is weakened, which is related to the previous antifungal activity (Fig. 2B). Tyrosol is upregulated after treatment with both emulsions, and tyrosol can change membrane permeability, allowing proteins, nucleic acids, and other contents to flow out and kill the fungus [40].

Some metabolites were found in the NEO treatment group: L-tyrosine, 3,4-dihydroxyphenylacetic acid, tyrosol, D-trehalose, DL-glyceric acid, and D-sucrose, among which all metabolites were downregulated except tyrosol. Fungal spore germination requires specific sugar molecules such as D-mannose, D-trehalose and D-xylose to trigger the "spore germinator" to enable spore germination [41, 42]. However, after NEO treatment, the amount of D-trehalose in *F. solani* significantly decreased (Additional file 1: Fig. S10B), which greatly reduced the germination rate of fungal spores, which was consistent with the results in Fig. 2B.

However, in the TEO treatment group, we observed that some metabolites, such as riboflavin, N6-(2-hydroxyethyl) adenosine, and isocitrate, were associated with multiple genes. After TEO treatment, riboflavin and N6-(2-hydroxyethyl) adenosine were upregulated, while isocitrate was downregulated. Riboflavin, also known as vitamin B_2, inactivates filamentous fungal cells [42], while N6-(2-hydroxyethyl) adenosine is a calcium antagonist that attenuates hydrogen peroxide-induced cellular oxidative toxicity [42], and isocitric acid is an intermediate in the TCA cycle. Its downregulation affects the TCA cycle of fungi and thus affects the life activities of fungi.

Finally, we found that the TCA cycle was greatly changed after two emulsion treatments (Fig. 8). After NEO and TEO treatment, the expression of malate dehydrogenase (MDH1), ATP citrate (pre-S) lyase (ACKY), pyruvate dehydrogenase E1 component (aceE), and citrate dehydrogenase (IDH1) genes was coregulated. In addition to the above common enzymes, NEO also inhibited the expression of succinate dehydrogenase (SDHA), citrate synthase (CS), and dihydrothioamide dehydrogenase (DLD) and upregulated the activity of fumaric acid hydratase (FH). In addition, the amount of phosphoenolpyruvate (PEP) was reduced, which affected the glycolysis/gluconeogenesis pathway. TEO upregulated the expression of genes encoding enzymes such as dihydrothioamide acetyltransferase (DLAT) and dihydrothioamide dehydrogenase (DLD) and inhibited aconitic acid hydratase (ACO), thereby reducing the amount of isocitrate.

In vitro and in vivo experiments of *P. notoginseng*

Previous experimental results show that NEO has a strong inhibitory effect on *F. solani* (Fig. 2). Therefore, to explore whether NEO has the same inhibitory effect on *F. solani* after acting on *P. notoginseng*, we inoculated *F. solani* on *P. notoginseng* and treated it with NEO. After 6 days of treatment, we observed that the fungal colonies in the roots of *P. notoginseng* inoculated with *F. solani* were dense and grew well, and the roots of *P. notoginseng* were obviously rotten, indicating that *F. solani* could infect *P. notoginseng* and cause the roots of *P. notoginseng* to rot. The lesion area of the *P. notoginseng* root slices inoculated with NEO (0.11 cm^2) was significantly smaller than that of the *P. notoginseng* slices inoculated with *F. solani* (0.58 cm^2) only (Fig. 9A, B).

At the same time, the in vivo experiment of *P. notoginseng* also showed the same results: the incidence and disease index of *P. notoginseng* seedlings inoculated with *F. solani* only were significantly higher than those of *P.*

(See figure on next page.)

Fig. 6 Transcriptome combined analysis with metabolome. **A** CK vs. NEO; **B** CK vs. TEO. The abscissa represents the enrichment factor (Diff/Background) of the pathway in different omics, and the ordinate represents the KEGG pathway name; the gradient of red–yellow–green represents the significant degree of enrichment from high–medium–low, expressed by *P* value; the shape of the bubble represents different omics, the circle is the gene, and the triangle is the metabolite; the size of bubbles represents the number of differential metabolites or genes. The larger the number is, the larger the point. All treatments were consistent with the above

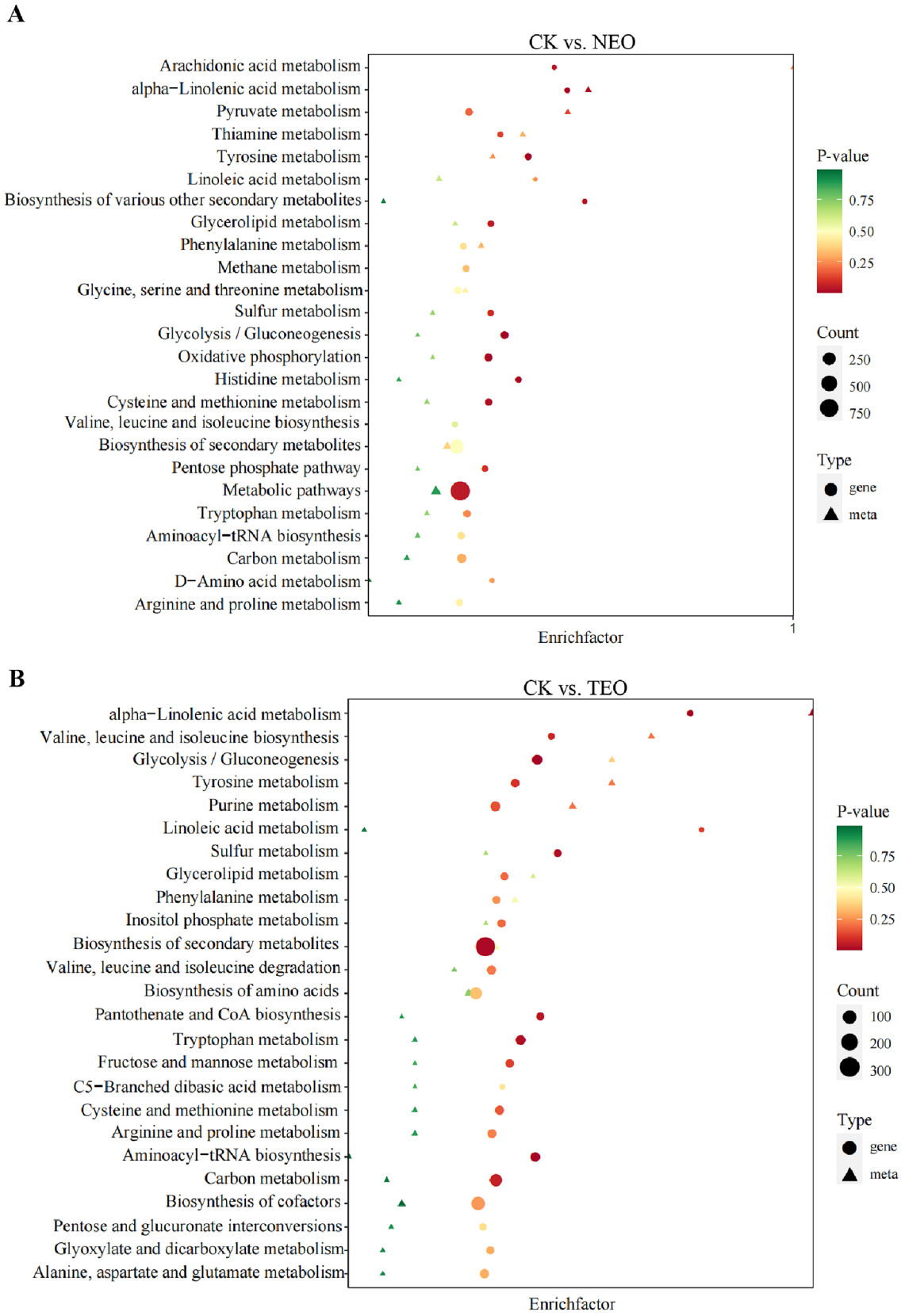

Fig. 6 (See legend on previous page.)

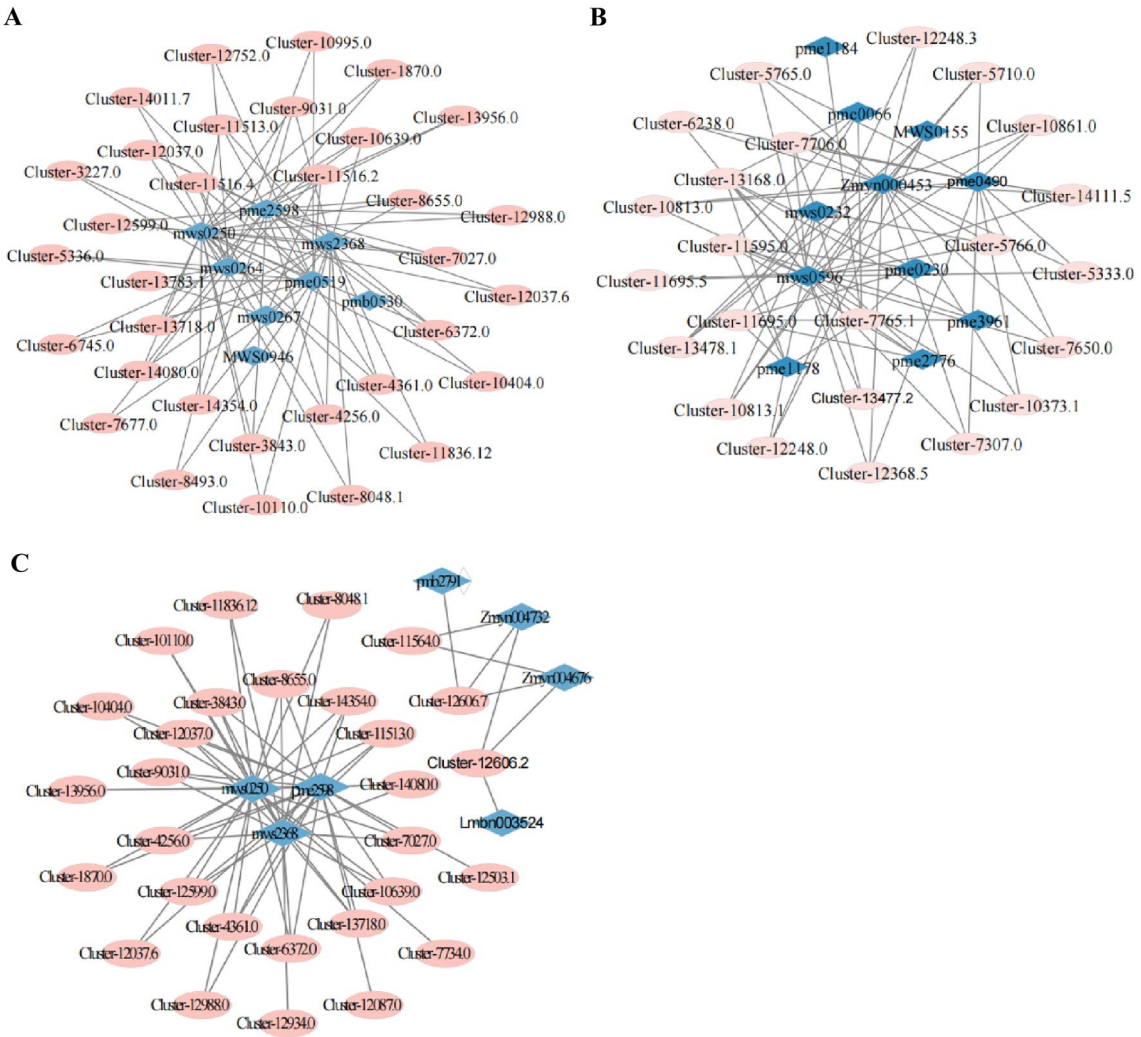

Fig. 7 Network analysis of DEGs and DAMs of *F. solani*. **A** Transcriptome and metabolome network diagram of NEO; **B** transcriptome and metabolome network diagram of TEO; **C** transcriptome and metabolome network diagram of the pathways shared by NEO and TEO. The pink ellipse represents genes, and the blue diamond represents metabolites

notoginseng seedlings inoculated with NEO. The chlorophyll content of *P. notoginseng* seedlings inoculated with NEO was higher than that of seedlings inoculated with *F. solani* only. These results show that NEO still maintains high antifungal activity after being applied to *P. notoginseng* and is expected to be developed as a new green pesticide.

The qRT-PCR verification of DEGs related to TCA cycle and meiosis

In order to verify the accuracy and repeatability of transcriptome analysis in this study, we performed qRT-PCR analysis of DEGs related to TCA cycle and meiosis. Among all candidate DEGs related to TCA cycle and meiosis, 9 genes were selected for qRT-PCR analysis. The Additional file 1: Fig. S11 shows the expression levels of 9 deg detected by qRT-PCR and RNA-Seq. In summary, the expression profiles of the 9 DEGs detected by qRT-PCR were consistent with the corresponding FPKM values obtained by RNA-Seq analysis. It shows that the expression data obtained by RNA-Seq in this study are reliable.

Discussion

EO is considered a weapon of phytochemical defense and an important source of green pesticides [43]. Previous studies have found that EO has an obvious inhibitory effect on a variety of pathogens causing *P. notoginseng* root rot [18]. However, in practical applications, EO cannot fully play its role due to its poor stability,

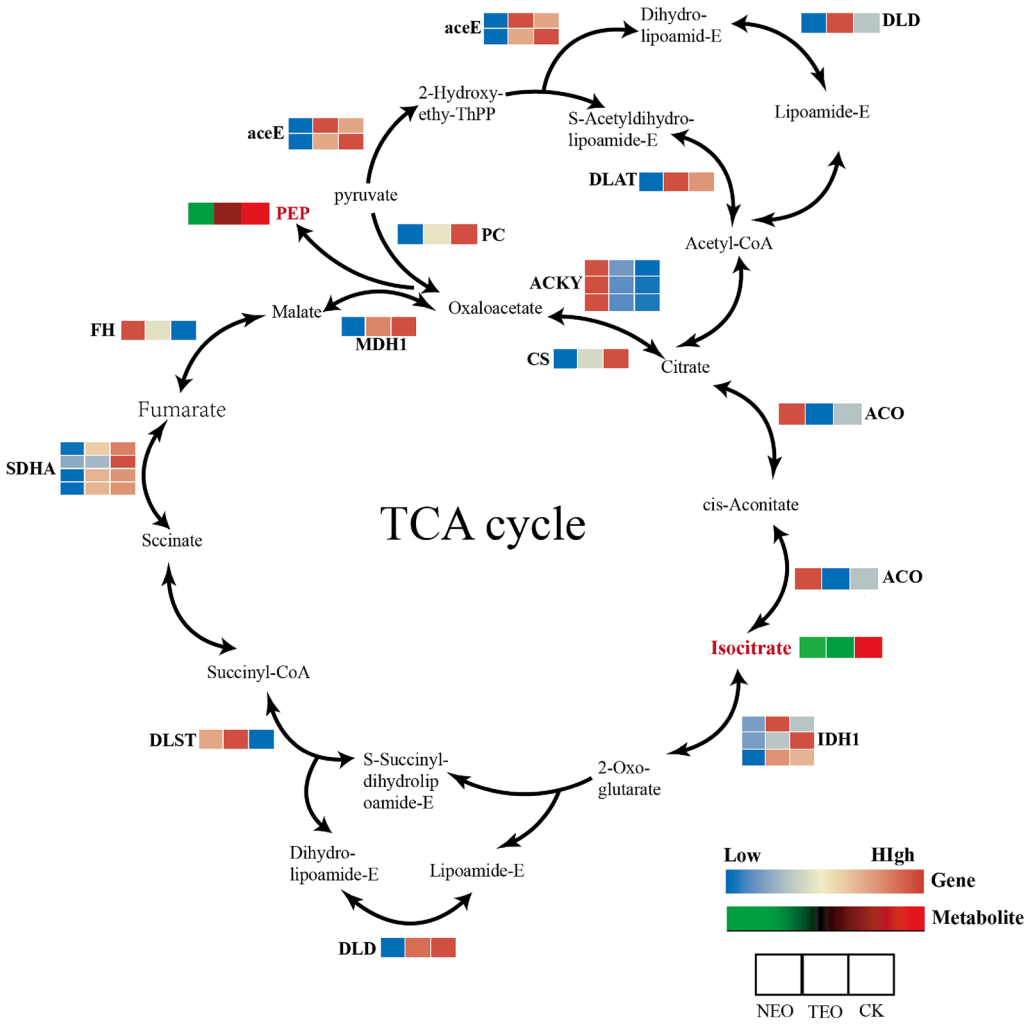

Fig. 8 The expression profiles of genes and metabolites related to the TCA cycle in the NEO treatment group and TEO treatment group. The DEGs and DAMs are presented in the form of a heatmap at the corresponding position of the gene or metabolite. The differential genes were blue (low) and red (high), and the differential metabolites were green (low) and red (high)

hydrophobicity, easy sedimentation, and coalescence. As a new type of delivery system, nanoemulsions greatly solve the above problems. Compared with ordinary emulsions, nanoemulsions have higher solubilization capacity and greater kinetic stability [44]. Some experiments have shown that the use of delivery systems at the nanoscale may enhance the passive transport of cells, thereby reducing mass transfer resistance and increasing antifungal activity. For example, the micelle-based system increases the antifungal activity of eugenol and carvacrol [45], and the microemulsion system can improve the activity of plant phenols [46]. In this study, EO was made into an oil-in-water nanoemulsion with an average particle size of 15.86 ± 1.96 nm by high-energy emulsification (Figs. 1, 10). Compared with TEO, the NEO we prepared can be miscible with water, and its particle size is reduced by 30 times, while the MIC is increased by 8 times (Fig. 2), and it remains stable in adverse environments such as high temperature, strong light, and high speed (Additional file 1: Figs. S2, S3). Therefore, the small particle size and strong stability are among the reasons why NEO has a stronger antifungal effect than TEO.

The reason why plant EO has antifungal activity is that EO has a variety of chemical components. The main active components of plant EO can be divided into three categories, namely, phenols, terpenes, and aldehydes [47]. Some work reports that all three components act mainly on the plasma membrane [47–49]. GC–MS detection of NEO and TEO showed that NEO contained phenols, terpenes, and aldehydes, which were 7.353%, 19.026%, and 35.275%, respectively. The contents of the three components in TEO were 0.785%, 18.615%, and 16.775% (Additional file 1: Fig. S4), respectively. Phenolic compounds showed the highest antifungal activity in EO

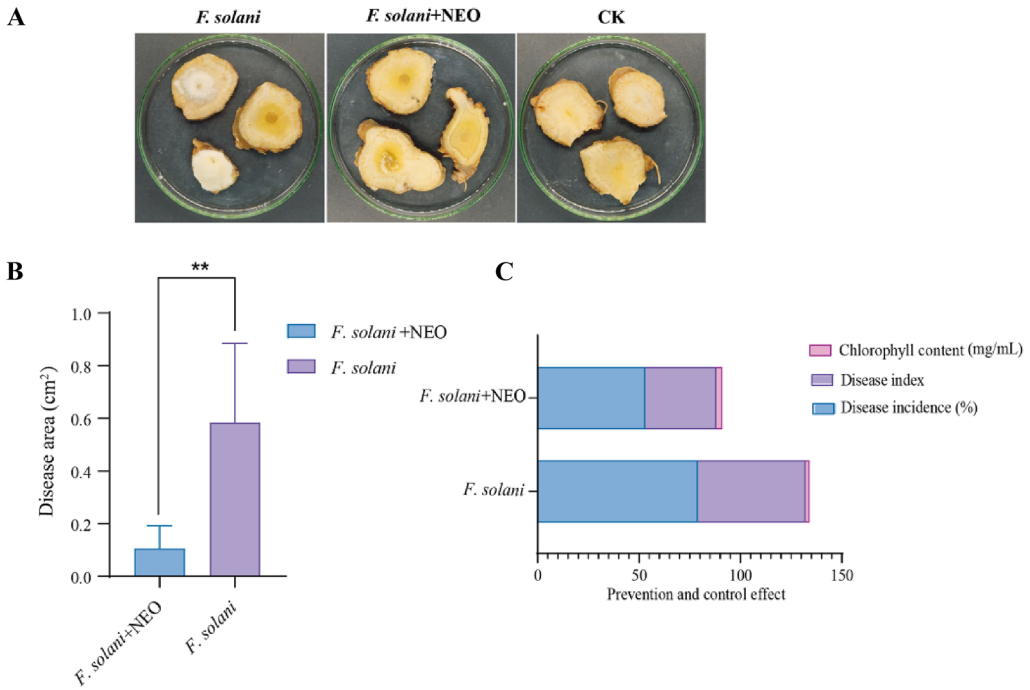

Fig. 9 The control effect of NEO on the infection of *F. solani* in *P. notoginseng* seedlings and their roots. **A**, **B** The control effect of NEO on isolated roots of *P. notoginseng*; **C** The control effect of NEO on root rot of *P. notoginseng* seedlings caused by *F. solani*. The data are expressed as the mean ± SD of three biological replicates

components [50]. The antifungal mechanism of terpenes may be accumulation in the cell membrane, leading to the loss of membrane integrity, the inhibition of respiratory enzymes, and the dissipation of proton power [51]. The potential target of aldehyde antimicrobial drugs is that membrane functional proteins that cause changes in membrane permeability can cause severe disturbances in the lipid part of the plasma membrane, resulting in changes in membrane permeability characteristics and leakage of intracellular substances [52]. The NEO we prepared greatly preserved the chemical composition of the EO, and the contents of phenols, terpenes, and aldehydes in the NEO were higher than those in the TEO (Additional file 1: Fig. S4). Some components that have been reported to have strong antimicrobial activity include citronellyl acetate [52], geranyl acetate [29], and linalool [53]. The content of NEO is higher than that of TEO, and NEO also contains additional antifungal components such as citral [54] and eugenol [55]. This shows that the increase in the content of antimicrobial components is the second reason why NEO has stronger antifungal activity than TEO. The results of transcriptome and metabolomics showed that both the NEO and TEO treatment groups entered the interior of fungal cells by destroying the fungal cell wall and cell membrane, further destroying ribosomes, the TCA cycle, and meiosis of fungi, thus inhibiting or even killing fungi.

The cell membrane is rich in glycerol, phospholipids, and sphingolipids, which play an important role in cell function and signal transduction pathways and are important organelles for fungi to resist external damage [56]. GO results showed that, compared with the TEO treatment group, NEO treatment showed more significant enrichment of differential genes in sphingolipid metabolism, membrane lipid decomposition, and cellular lipid decomposition (Additional file 1: Fig. S6). Metabolome results showed that components related to the cell membrane decreased after NEO and TEO treatment (Additional file 1: Fig. S10A). These results indicate that both NEO and TEO can cause cell membrane damage, and the damage degree of NEO is deeper. The reason why NEO damages cell membranes more deeply may be related to the higher amounts of phenols, terpenes, and aldehydes contained in NEO. Lipids are fundamental molecules that provide a variety of structures and signal transduction functions in a variety of organisms. There is considerable evidence that plasma membrane lipids are important regulators of fungal pathogenicity [57]. Various glycolipids have been shown to have toxic properties in several fungal species, while others have been shown to play a role in host defense. In addition to their role

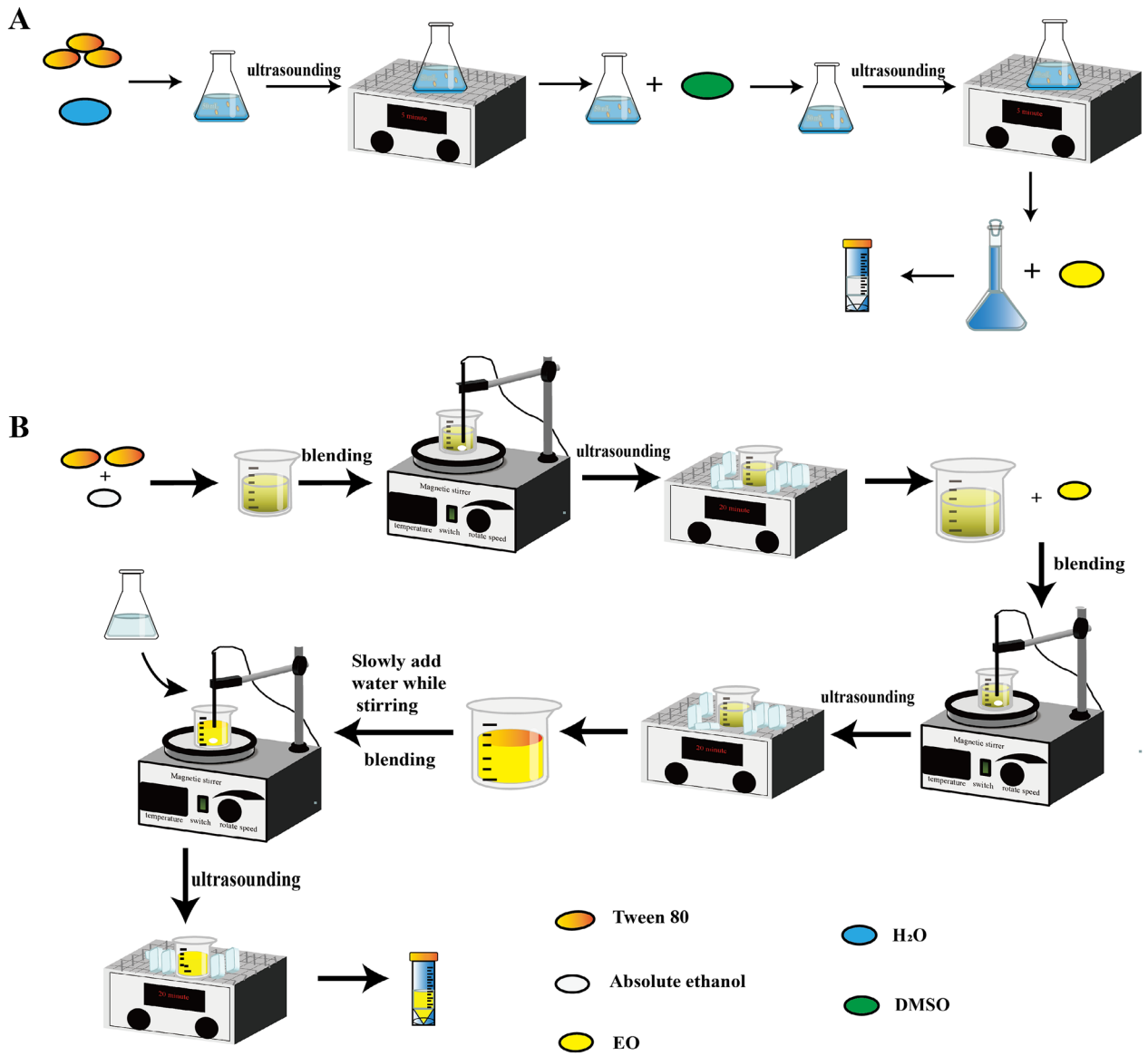

Fig. 10 Two kinds of emulsion preparation flow chart. **A** TEO preparation flow chart. We used 1/1000 Tween-80 and 20/1000 DMSO to prepare TEO; **B** NEO preparation flow chart. The ratio of Tween-80 to anhydrous ethanol was 2:1, and the ratio of mixed surfactant to EO was 4:1

as virulence agents, lipids contribute to other virulence mechanisms, such as drug resistance, biofilm formation, and extracellular vesicle release [58]. Therefore, the cell membrane can be used as an anti-*F. solani* target for further research.

Ribosomes are mainly composed of rRNA and proteins, which are highly conserved during evolution. Ribosomes play an important role in cell composition and energy metabolism. Studies have shown that 70–90% of cell energy metabolism consumes and connects related genes of 9 common metabolites into the ribosome mechanism, indicating the coevolution between cell composition and energy [59]. In addition, the ribosome is the main site of protein synthesis and the core of the translation mechanism. If the ribosome stops translation before reaching the stop codon, resulting in its inability to dissociate from mRNA in time, it will produce truncated peptides. These polypeptide chains are likely to cause cell carcinogenesis [60]. The GO and KEGG results showed that the differentially expressed genes related to ribosomes were significantly enriched after NEO and TEO treatment, and the number of differentially expressed genes in the NEO treatment group was greater than that in the TEO treatment group (Fig. 4, Additional file 1: Fig. S6). In

this study, *F. solani* treated with NEO and TEO caused a strong inhibition of ribosomal protein translation, which led to a serious impact on the growth and development of *F. solani*.

The TCA cycle is the core process of all biological substances and energy metabolism. It is the most effective way for the body to oxidize sugars or other substances to obtain energy. It is the hub of metabolism, communication and transformation of sugars, lipids, proteins, and even nucleic acids [61]. The combined analysis of the transcriptome and metabolome found that both the NEO and TEO treatment groups changed the enzymes and metabolites in the TCA cycle, causing metabolic disorders in *F. solani*, thereby affecting the spore germination and mycelial growth of *F. solani*, and the degree of damage in the NEO treatment group was greater than that in the TEO treatment group (Fig. 8). This is consistent with the previous phenotype (Fig. 2). Under NEO treatment, due to the destruction of the TCA cycle, *F. solani* maintains life activities against damage, so it resists NEO-induced cytotoxicity through oxidative enzymes, glutathione metabolism, and fatty acid biosynthesis and enhances the oxidative phosphorylation pathway to produce ATP for cell energy supply. The TEO treatment group upregulated the biosynthesis of secondary metabolites, amino acid biosynthesis (tryptophan, arginine, phenylalanine), amino-tRNA biosynthesis, and other pathways to enrich the synthesis of secondary metabolites and proteins to resist invasion.

Meiosis is a special form of nuclear division that usually leads to a reduction in chromosome number from diploid to haploid. Many enzymes in meiosis play a crucial role in fungal growth and spore germination [62]. After treatment with NEO and TEO, the expression of Bub1, RAD53, Ime2, and Snf1 was downregulated. Cells often employ a number of mechanisms to ensure that their genomes are replicated and separated with high fidelity in each cell cycle. Errors in chromosome segregation often lead to cell death [32]. During mitosis, spindle checkpoints monitor kinematic–microtubule interactions and can only proceed later if all sister chromatid pairs achieve bidirectional orientation on the mitotic spindle. Bub1 is a fission yeast centromere scaffold protein sufficient to recruit other spindle checkpoint proteins to ectopic sites on chromosomes, and Rad53 kinase plays a central role in yeast DNA damage checkpoints [33, 63]. The decrease in Bub1 and Pad53 expression will make the genome of fungal cells unable to replicate and separate with high fidelity, resulting in cell death. Ime1 is required for the initiation of meiosis, which is regulated by Snf1 kinase. The former activates G1-to-S conversion, and the latter mediates glucose inhibition. The meiosis and sporulation of yeast depend on (1) starvation of at least one essential nutrient, such as nitrogen, sulfur, or phosphorus, (2) the presence of nonfermentable carbon sources, such as acetate, and (3) glucose deficiency [64]. These three conditions must be met before the cell enters the meiosis pathway; the downregulation of genes controlling Snf1 kinase leads to the failure of meiosis and conidiation [34]. Ime2 belongs to a conserved protein kinase family, which is similar to the sequence of cyclin-independent kinase and mitogen-activated protein kinase. Ime2 plays a key role in meiosis and sporulation. This protein kinase is involved in the regulation of various key events in meiosis, such as the initiation of DNA replication and the regulation of meiosis-specific gene expression. It has been reported that downregulation or deletion of Ime2 expression inhibits the mycelial growth of fungi (*F. oxysporum*) and reduces their sporulation [65]. The decrease in Snf1 and Ime2 kinase expression is an important reason for the decrease in spore germination and mycelial growth in the NEO treatment group and TEO treatment group. The genes controlling Snf1 and Ime2 enzymes were downregulated more in the NEO treatment group than in the TEO treatment group, which may be one of the reasons why the NEO treatment group had stronger antifungal activity.

As a new delivery system, nanoemulsions not only solve the problem of low bioavailability of traditional emulsions but also greatly enhance their antifungal activity. In this paper, the antifungal mechanism of NEO was preliminarily explored. In the future, the corresponding targets can be located for further antifungal research.

Conclusions

The NEO prepared in this study is an oil-in-water nanoemulsion with a particle size of 15.86 ± 1.96 nm and strong stability. Compared with TEO, its antifungal effect is better, and the relative content of antifungal components increases and still maintains good antifungal activity after acting on *P. notoginseng*. From the transcriptome and metabolome results, we know that both TEO and NEO inhibit *F. solani* by destroying the cell wall and cell membrane of fungi, thereby destroying the ribosomes of fungi and affecting the TCA cycle and meiosis of fungi (Fig. 11). It is worth noting that the damage degree of the NEO treatment group was higher than that of the TEO treatment group. At the same time, we found that some key enzymes related to mycelial growth and spore germination, such as Ime2 and Snf1, and some metabolites, such as D-trehalose, L-tyrosine, 3,4-dihydroxyphenylacetic acid, and tyrosol, were higher in the NEO treatment group than in the TEO treatment group. In summary, this study not only solved the problems of EO insoluble in water and low bioavailability but also greatly improved the antifungal

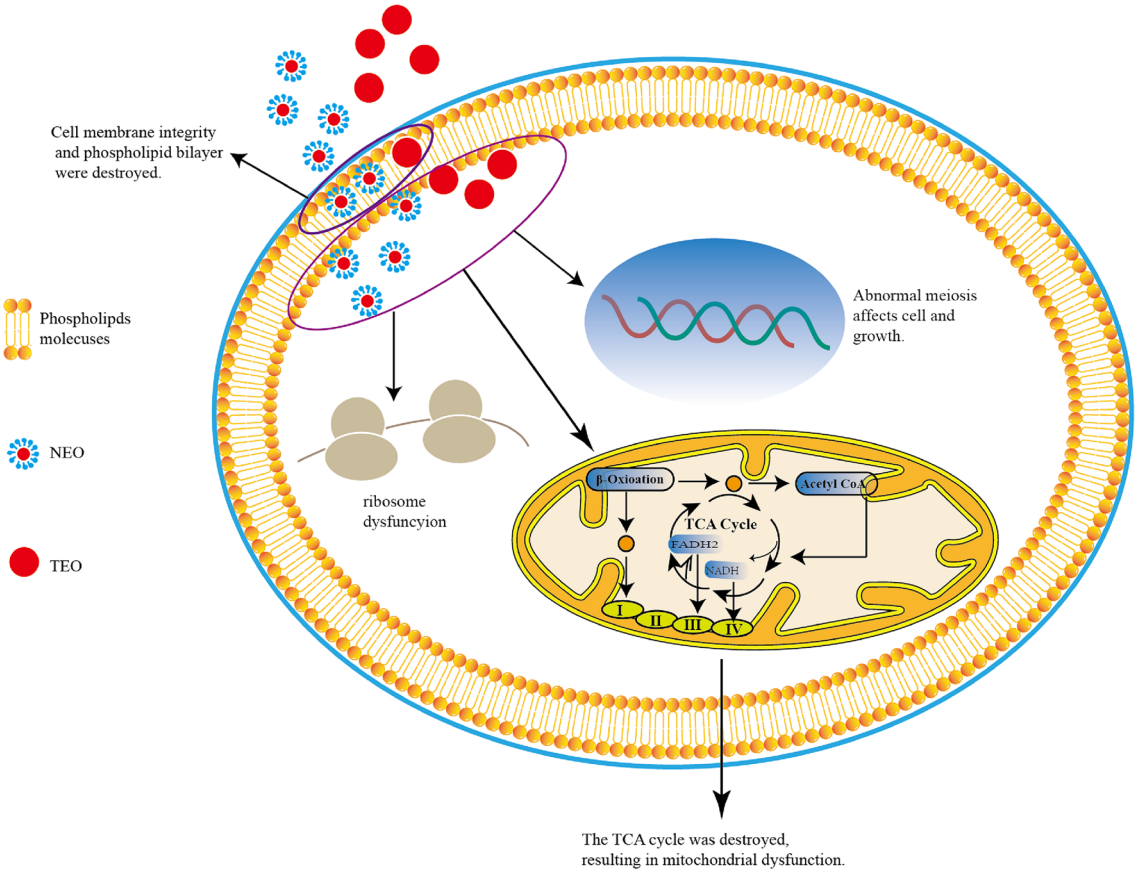

Fig. 11 The mechanism overview of NEO and TEO on *F. solani*

activity, revealing the antifungal mechanism and the reason for the enhancement of NEO activity. It provides theoretical research for further development and utilization of EO to produce environmentally friendly pesticides or fertilizers and alleviate root rot of medicinal plants.

Abbreviations

EO	*Cymbopogon citratus* (DC.) Stapf essential oil
NEO	*Cymbopogon citratus* (DC.) Stapf nanoemulsion
TEO	*Cymbopogon citratus* (DC.) Stapf traditional emulsion
GC–MS	Chemical composition analysis by gas chromatography–mass spectrometry
DMSO	Dimethyl sulfoxide
Km	Ratio of surfactant to cosurfactant
MIC	The minimum inhibitory concentration
DEGs	Differentially expressed genes
DAMs	Differential metabolites

Supplementary Information

The online version contains supplementary material available at https://doi.org/10.1186/s40538-023-00511-7.

Additional file 1: Fig. S1. Effect of mixing Tween-80 and anhydrous ethanol at different Km values on the ternary phase diagram of the nanoemulsion. The best Km was selected by the area of the blue part. **Fig. S2.** NEO stability test. NEO under different (A) temperatures; (B) salt concentrations; (C) rotational speeds for 15 min; (D) effect of different pH values on the stability of NEO; (E) effects of different illuminations on nanoemulsions. The bars represent ± SD for three independent biological experiments. **Fig. S3.** The antifungal activity of different light intensities on NEO treatment after 48 h. (A) Inhibition growth curve of *F. solani* after different NEO treatments. (B) Growth to the seventh day, the opposite of *F. solani*. The data are expressed as the mean ± standard deviation of three biological replicates. **Fig. S4.** Chemical composition of the two emulsions. (A) Chemical composition of EO; (B) Chemical composition of NEO. (C) Chemical composition of TEO. The values are presented as the mean of three replicates. **Fig. S5.** Transcriptome analysis of *F. solani* treated with NEO and TEO; (A) PCA plots of differential gene expression; (B) CK vs. TEO, CK vs. NEO intercomparison of differential gene Venn diagram; Differential genetic volcano map of (C) NEO; (D) TEO. Each dot in the volcano plot denotes one gene. The green spots denote genes with downregulated differential expression; the red spots denote genes with upregulated differential expression; the gray spots denote the detected genes without significant differences. All treatments were consistent with the above. **Fig. S6.** GO enrichment analysis of DEGs in CK vs. NEO (A) and in CK vs. TEO (B), including biological process, cellular component, and molecular function. The horizontal axis represents the degree of enrichment, the vertical axis represents the functional classification, the bubble size represents the number of genes, and the bubble color represents the enrichment significance p value. All treatments were consistent with the above. **Fig. S7.** (A) Changes in related genes during meiosis. (B) Expression of ribosome-related genes. **Fig. S8.** Extensive targeted metabolomic analysis of *F. solani* treated with NEO and TEO. (A) Metabolite PCA graph; (B) histogram of up- and downregulated differential metabolites from pairwise comparisons;

(C) differential metabolites upregulated in the comparison of CK vs. TEO and CK vs. NEO; (D) differential metabolites downregulated in the comparison of CK vs. TEO and CK vs. NEO. **Fig. S9.** The top 20 KEGG pathways enriched by DAMs. (A) DAMs of CK vs. NEO; (B) DAMs of CK vs. TEO. The X-axis is the enrichment factor, and the Y-axis represents the name of the pathway. The bubble size represents the number of DAMs involved. The bubble color indicates the enrichment degree of the pathway. All treatments were consistent with the above. **Fig. S10.** Amount of key metabolites: (A) Metabolites associated with cell membrane composition; (B) the amount of D-trehalose; (C) the amount of key metabolites in the network diagram. All treatments were consistent with the above. **Fig. S11.** A total of 9 genes were screened by qRT-PCR verification of TCA cycle and meiosis-related genes. The ratio of qPCR expression to CK expression was calculated as 1.

Acknowledgements
Not applicable.

Author contributions
X.D. conceived the original idea. J.W. wrote the manuscript. J.W., H. L., and H.N. performed the experiments. C.L. and L.Z. analyzed data. F.X. commented the manuscript. X.D. wrote the paper and discussed it with all authors. All the authors read and approved the final manuscript.

Funding
This work was funded by the National Natural Science Foundation of China (82060683), Yunnan Provincial Science and Technology Plan-Basic Research Project (202301AW070008), Wang Yuan Chao Expert Workstation in Yunnan Province (202305AF150018), Yunnan Provincial Science and Technology Department-Applied Basic Research Joint Special Funds of Yunnan University of Traditional Chinese Medicine (202101AZ070001-047), and Yunnan Provincial Key Laboratory for Sustainable Utilization of Southern Medicine (202105AG070012XS23012).

Availability of data and materials
The original contributions presented in this study are included in the article/Supplementary material, and further inquiries can be directed to the corresponding author.

Declarations

Competing interests
The authors declare that they have no competing interest.

Author details
[1]School of Chinese Materia Medica, Yunnan University of Chinese Medicine, Kunming 650500, China.

Received: 31 October 2023 Accepted: 21 November 2023
Published online: 07 December 2023

References

1. Wang XC, Xiong XJ, Wang H, Wang J. Protective effects of *panax notoginseng* saponins on cardiovascular diseases: a comprehensive overview of experimental studies. Evid-Based Compl Alt. 2014. https://doi.org/10.1155/2014/204840.
2. Zhang ZL, Wang WQ, Wang Y, Yang JZ, Cui XM. Influence of *panax notoginseng* continuous cropping on seed germination and seedling growth of the plant. Chin J Plant Ecol. 2010;29:1493–7.
3. Li J, Bao Y, Wang Z, Yang Q, Cui X. Research progress in diseases of *panax notoginseng*. Physiol Mol Plant P. 2022. https://doi.org/10.1016/j.pmpp.2022.202878.
4. Miao ZQ, Li SD, Liu XZ, Chen YJ, Zhang KQ. The causal microorganisms of *panax notoginseng* root rot disease. Zhongguo Nong Ye Ke Xue. 2006;39:1371–8.
5. Zhou LH, Han Y, Ji GH, Wang ZS, Liu F. First report of bacterial leaf spot disease caused by pseudomonas syringae pv syringae on *panax notoginseng*. Plant Dis. 2013. https://doi.org/10.1094/PDIS-11-12-1047-PDN.
6. Lan Y, Shi L, Li X. Occurrence of root rot of *panax notoginseng* caused by *Fusarium oxysporum* in China. Int J Agric Biol. 2018. https://doi.org/10.17957/IJAB/15.0757.
7. Deng J, Guan R, Liang T, Su L, Ge F, Liu D. Dirigent gene family is involved in the molecular interaction between *panax notoginseng* and root rot pathogen *Fusarium solani*. Ind Crops Prod. 2022. https://doi.org/10.1016/j.indcrop.2022.CuiX,114544.
8. Peng F, Zhang MY, Hou SY, Chen J, Wu YY, Zhang YX. Insights into streptomyces spp. isolated from the rhizospheric soil of *panax notoginseng*: isolation, antimicrobial activity and biosynthetic potential for polyketides and non-ribosomal peptides. BMC Microbiol. 2020. https://doi.org/10.1186/s12866-020-01832-5.
9. Li Z, He C, Wang C, Cui X, Yu S, Luo W. Studies on control of root rot on *panax notoginseng*. China J Chin Mater Med. 1998;21:163–6.
10. Shahid M, Khan MS. Ecotoxicological implications of residual pesticides to beneficial soil bacteria: a review. Pest Biochem Physiol. 2022. https://doi.org/10.1016/j.pestbp.2022.105272.
11. Bolouri P, Salami R, Kouhi S, Kordi M, Asgari Lajayer B, Astatkie T, et al. Applications of essential oils and plant extracts in different industries. Molecules. 2022. https://doi.org/10.3390/molecules27248999.
12. Chen CJ, Li QQ, Ma YN, Wang W, Cheng YX, Dong X, et al. Antifungal effect of essential oils from five kinds of rutaceae plants—avoiding pesticide residue and resistance. Chem Biodivers. 2019. https://doi.org/10.1002/cbdv.201800688.
13. Verma M, Sharma S. Antifungal activity of four plant essential oils against phytopathogenic fungi *Fusarium oxysporum*. J Biosci Bioeng. 2017. https://doi.org/10.1016/j.jbiosc.2016.09.011.
14. Yang J, Li TT, Huo YY, Huang HY, Meng QH, Dong X, et al. *Cymbopogom Citratus* essential oils: a promising source of antifungals against *panax notoginseng*-associated pathogenic fungi. Curr Microbiol. 2022. https://doi.org/10.1007/s00284-022-03119-6.
15. Singh Y, Meher JG, Raval K, Khan FA, Chaurasia M, Chourasia MK, et al. Nanoemulsion: concepts, development and applications in drug delivery. J Control Release. 2017. https://doi.org/10.1016/j.jconrel.2017.03.008.
16. Almotwaa S. Coupling Ifosfamide to nanoemulsion-based clove oil enhances its toxicity on malignant breast cancer and cervical cancer cells. Pharmacia. 2021. https://doi.org/10.3897/pharmacia.68.e68291.
17. Feng JG. Application of nanoemulsions in formulation of pesticides. Nanoemulsions. 2018. https://doi.org/10.1016/B978-0-12-811838-2.00012-6.
18. Yin YJ, Chen CJ, Guo SW, Li KM, Ma YN, Sun WM, et al. The fight against *panax notoginseng* root-rot disease using zingiberaceae essential oils as potential weapons. Front Plant Sci. 2018. https://doi.org/10.3389/fpls.2018.013469:1346.
19. Sun WM, Ma YN, Yin YJ, Chen CJ, Cheng YX. Effects of essential oils from zingiberaceae plants on root-rot disease of *panax notoginseng*. Molecules. 2018. https://doi.org/10.3390/molecules23051021.
20. Lotfi M, Moghadamnia AA. Nanoemulsions: techniques for the preparation and the recent advances in their food applications. Innov Food Sci Emerg. 2022. https://doi.org/10.1016/j.ifset.2021.102914.
21. Tubesha Z, Bakar ZA, Ismail M. Characterization and stability evaluation of thymoquinone nanoemulsions prepared by high-pressure homogenization. J Nanomater. 2013. https://doi.org/10.1155/2013/453290.
22. Zeng ZY, Li QQ, Huo YY, Chen CJ, Duan SS, Dong X, et al. Inhibitory effects of essential oils from Asteraceae plant against pathogenic fungi of *Panax notoginseng*. J Appl Microbiol. 2021. https://doi.org/10.1111/jam.14606.
23. Zhang YM, Cheng YX, Ma YN, Chen CJ, Xv FR, Dong X. Role of phenolic acids from the rhizosphere soils of *panax notoginseng* as a double-edge sword in the occurrence of root-rot disease. Molecules. 2018. https://doi.org/10.3390/molecules23040819.
24. Liu XY, Huo YY, Yang J, Li TT, Xu FR, Dong X, et al. Integrated physiological, metabolomic, and proteome analysis of Alpinia officinarum Hance essential oil inhibits the growth of *Fusarium oxysporum* of *panax notoginseng*. Front Microbiol. 2022. https://doi.org/10.3389/fmicb.2022.1031474.
25. Li QQ, Huo YY, Chen CJ, Zeng ZY, Xu FR, Dong X, et al. Biological activities of two essential oils from pogostemon cablin and eupatorium fortunei

and their major components against fungi isolated from *panax notoginseng*. Chem Biodivers. 2020. https://doi.org/10.1002/cbdv.202000520.
26. Sajjadi S. Nanoemulsion formation by phase inversion emulsification: on the nature of inversion. Colloids Surf. 2006. https://doi.org/10.1021/la060043e.
27. Maatooq GT, Hoffmann JJ. Microbiological conversion of a beta- and gamma-eudesmol mixture by Rhizopus. Pharmazie. 2002. https://doi.org/10.1051/vetres:2006032.
28. Mota DL, Samara K, Mendes MJ, Oliveira D, Oliveira I, et al. Antifungal activity of geraniol and citronellol, two monoterpenes alcohols, against Trichophyton rubrum involves inhibition of ergosterol biosynthesis. Pharm Biol. 2015. https://doi.org/10.3109/13880209.2014.913299.
29. Khayyat SA, Sameeh MY. Bioactive epoxides and hydroperoxides derived from naturally monoterpene geranyl acetate. Saudi Pharm J. 2018. https://doi.org/10.1016/j.jsps.2017.11.005.
30. Morris C, Cluet D, Ricci EP. Ribosome dynamics and mRNA turnover, a complex relationship under constant cellular scrutiny. WIREs RNA. 2021. https://doi.org/10.1002/wrna.1658.
31. Puryear R, Macech P, Yazawa I. Complete solution for TCA cycle organic acid analysis. LC GC N AM. 2019;32:37–715.
32. Rischitor PE, May KM, Hardwick KG. Bub1 is a fission yeast kinetochore scaffold protein, and is sufficient to recruit other spindle checkpoint proteins to ectopic sites on chromosomes. PLoS ONE. 2007. https://doi.org/10.1371/journal.pone.0001342.
33. Pike BL, Yongkiettrakul S, Tsai M-D, Heierhorst J. Mdt1, a novel Rad53 FHA1 domain-interacting protein, modulates DNA damage tolerance and G2/M Cell cycle progression in Saccharomyces cerevisiae. Mol Cell Biol. 2004. https://doi.org/10.1128/MCB.24.7.2779-2788.2004.
34. Purnapatre K, Piccirillo S, Schneider BL, Honigberg SM. The CLN3/SWI6/CLN2 pathway and SNF1 act sequentially to regulate meiotic initiation in Saccharomyces cerevisiae. Genes Cells. 2002. https://doi.org/10.1046/j.1365-2443.2002.00551.
35. Irniger S. The Ime2 protein kinase family in fungi: more duties than just meiosis. Mol Microbiol. 2011. https://doi.org/10.1111/j.1365-2958.2011.07575.
36. Burch JM, Mashayekh S, Wykoff DD, Grimes CL. Bacterial derived carbohydrates bind Cyr1 and trigger hyphal growth in Candida albicans. ACS Infect Dis. 2018. https://doi.org/10.1021/acsinfecdis.7b00154.
37. Noda S, Shirai T, Mochida K, Matsuda F, Oyama S, Kondo A, et al. Evaluation of brachypodium distachyon L-Tyrosine decarboxylase using L-Tyrosine over-producing saccharomyces cerevisiae. PLoS ONE. 2015. https://doi.org/10.1371/journal.pone.0125488.
38. Harris DM, Diderich JA, Krogt Z, Luttik M, Pronk JT. Enzymic analysis of NADPH metabolism in β-lactam-producing Penicillium chrysogenum: presence of a mitochondrial NADPH dehydrogenase. Metab Eng. 2006. https://doi.org/10.1016/j.ymben.2005.09.004.
39. Fernandes C, Mota M, Barros L, Dias MI, Ferreira I, Gonçalves T, et al. Pyomelanin synthesis in alternaria alternata inhibits DHN-melanin synthesis and decreases cell wall chitin content and thickness. Front Microbiol. 2021. https://doi.org/10.3389/fmicb.2021.691433.
40. Sebaa S, Boucherit-Otmani Z, Courtois P. Effects of tyrosol and farnesol on Candida albicans biofilm. Mol Med Rep. 2019. https://doi.org/10.3892/mmr.2019.9981.
41. Liu H, Yang S, Wang X, Wang T. Production of trehalose with trehalose synthase expressed and displayed on the surface of Bacillus subtilis spores. Microb Cell Factories. 2019. https://doi.org/10.1186/s12934-019-1152-7.
42. Kashiwabuchi RT, Carvalho FRS, Khan YA, Hirai F, Campos MS, McDonnell PJ. Assessment of fungal viability after long-wave ultraviolet light irradiation combined with riboflavin administration. Graef Arch Clin Exp. 2013. https://doi.org/10.1007/s00417-012-2209-z.
43. Mohan M, Haider SZ, Andola HC, Purohit VK. Essential oils as green pesticides: for sustainable agriculture. RJPBCS. 2011;2:100–6.
44. Donsì F, Annunziata M, Vincensi M, Ferrari G. Design of nanoemulsion-based delivery systems of natural antimicrobials: effect of the emulsifier. J Biotechnol. 2012. https://doi.org/10.1016/j.jbiotec.2011.07.001.
45. Liolios CC, Gortzi O, Lalas S, Tsaknis J, Chinou I. Liposomal incorporation of carvacrol and thymol isolated from the essential oil of origanum dictamnus L. and in vitro antimicrobial activity. Food Chem. 2009. https://doi.org/10.1016/j.foodchem.2008.05.060.
46. Gortzi O, Lalas S, Chinou I, Tsaknis J. Reevaluation of bioactivity and antioxidant activity of Myrtus communis extract before and after encapsulation in liposomes. Eur Food Res Technol. 2007. https://doi.org/10.1007/s00217-007-0592-1.
47. Ceylan E, Fung D. Antimicrobial activity of spices 1. J Rapid Meth Aut Mic. 2010. https://doi.org/10.1111/j.1745-4581.2004.tb00046.
48. Sikkema J, Debont J, Poolman B. Interactions of cyclic hydrocarbons with biological membranes. J Biol CHEM. 1994. https://doi.org/10.0000/PMID8132524.
49. Ultee A, Bennik MHJ, Moezelaar R. The phenolic hydroxyl group of carvacrol is essential for action against the food-borne pathogen bacillus cereus. AEM. 2002. https://doi.org/10.1128/AEM.68.4.1561-1568.
50. Burt SA. Essential oils: their antibacterial properties and potential applications in foods—a review. Int J Food Microbiol. 2004. https://doi.org/10.1016/j.ijfoodmicro.2004.03.02.
51. Pasqua RD, Betts G, Hoskins N, Edwards M, Mauriello G. Membrane toxicity of antimicrobial compounds from essential oils. J Agric Food Chem. 2007. https://doi.org/10.1021/jf0636465.
52. Lambert RJW, Skandamis PN, Coote PJ, Nychas G. A study of the minimum inhibitory concentration and mode of action of oregano essential oil, thymol and carvacrol. J Appl Microbiol. 2010. https://doi.org/10.1046/j.1365-2672.2001.01428.
53. El-Baky R, Hashem ZS. Eugenol and linalool: comparison of their antibacterial and antifungal activities. Afr J Microbiol. 2016. https://doi.org/10.5897/AJMR2016.8283.
54. Cristiane D, Silva S, Guterres I, Vanessa W, Schapobal EES. Antifungal activity of the lemongrass oil and citral against Candida Sepses. Braz J Infect Dis. 2008. https://doi.org/10.1590/s1413-86702008000100014.
55. Yang R, Miao J, Shen Y, Cai N, Chen J. Antifungal effect of Cinnamaldehyde, Eugenol and Carvacrol nanoemulsion against Penicillium digitatum and application in postharvest preservation of citrus fruit. LWT. 2021. https://doi.org/10.1016/j.lwt.2021.110924.
56. Sant DG, Tupe SG, Ramana CV, Deshpande MV. Fungal cell membrane-promising drug target for antifungal therapy. J Appl Microbiol. 2016. https://doi.org/10.1111/jam.13301.
57. Rella A, Farnoud AM, Del Poeta M. Plasma membrane lipids and their role in fungal virulence. Prog Lipid Res. 2016. https://doi.org/10.1016/j.plipres.2015.11.003.
58. Tada R, Latge JP, Aimanianda V. Undressing the fungal cell wall/cell membrane—the antifungal drug targets. Curr Pharm Des. 2013. https://doi.org/10.2174/1381612811319200012.
59. Wang Z, Gaba A, Sachs MS. A highly conserved mechanism of regulated ribosome stalling mediated by fungal arginine attenuator peptides that appears independent of the charging status of arginyl-tRNAs. J Biol Chem. 1999. https://doi.org/10.1074/jbc.274.53.37565.
60. Russell PJ, Wilkerson WM. The structure and biosynthesis of fungal cytoplasmic ribosomes. Exp Mycol. 1980;4:281–337.
61. Kubicek CP. Regulatory aspects of the tricarboxylic acid cycle in filamentous fungi—a review. Trans Br Mycol Soc. 1988. https://doi.org/10.1016/S0007-1536(88)80141-4.
62. Heywood P, Magee PTJBR. Meiosis in protists: some structural and physiological aspects of meiosis in algae, fungi, and protozoa. Bacteriol Rev. 1976. https://doi.org/10.1128/br.40.1.190-240.1976.
63. Ouyang B, Knauf JA, Ain K, Nacev B, Fagin JA. Mechanisms of aneuploidy in thyroid cancer cell lines and tissues: evidence for mitotic checkpoint dysfunction without mutations in BUB1 and BUBR1. Clin Endocrinol. 2002. https://doi.org/10.1046/j.1365-2265.2002.01475.
64. Wendland J. Sporulation in Ashbya gossypii. J Fungi. 2020. https://doi.org/10.3390/jof6030157.
65. Xiao J, Zhang Y, Yang K, Tang Y, Wei L, Liu E, Liang Z. Protein kinase Ime2 is associated with mycelial growth, conidiation, osmoregulation, and pathogenicity in *Fusarium oxysporum*. Arch Microbiol. 2022. https://doi.org/10.1007/s00203-022-02964-0.

Publisher's Note